

On Models with Power Conservation in Reflective Intelligent Surfaces and their Design Implications

Robin J. Williams, Pablo Ramírez-Espinosa, Olena Semenovska and Petar Popovski

Abstract—Reconfigurable intelligent surfaces (RISs) are potential enablers of future wireless communications and sensing applications and use-cases. The RIS is envisioned as a dynamically controllable surface that is capable of transforming impinging electromagnetic waves in terms of angles and polarization. Many models has been proposed to predict the wave-transformation capabilities of potential RISs, where power conservation is ensured by enforcing that the scattered power equals the power impinging upon the aperture of the RIS, without considering whether the scattered field adds coherently or destructively with the source field. In effect, this means that power is not conserved, as elaborated in this paper. With the goal of investigating the implications of global and local power conservation in RISs, work considers a single-layer metasurface based RIS. A complete end-to-end communications channel is given through polarizability modeling and conditions for power conservation and channel reciprocity are derived. The implications of the power conservation conditions upon the end-to-end communications channel is analyzed.

Index Terms—Reconfigurable Intelligent Surface (RIS), metasurface, non-reciprocity, power conservation, channel estimation, scattering, radar cross section (RCS), mutual coupling, farfield, polarizability.

I. INTRODUCTION

The term Reflective intelligent surfaces (RISs), also called Reconfigurable Intelligent surfaces are used to refer to the electromagnetic surfaces that can be dynamically controlled to change the properties of the wireless propagation environment. Ideally, RISs are conceived as semi-passive electromagnetic sheets whose dynamic impact on the propagated waves can be advantageous in multiple ways, such as communication, sensing, positioning [1] or even control of electromagnetic exposure [2].

A model commonly used to capture the impact of RIS on the wireless propagation is the *cascaded channel model*, where a RIS is modeled as a collection of sub-wavelength reflecting elements, resulting in an equivalent channel at the receiver [3]:

$$\mathbf{H} = \mathbf{H}_1 \Phi \mathbf{H}_2, \quad (1)$$

where \mathbf{H}_1 is the channel matrix from the transmitter to the RIS, \mathbf{H}_2 is the channel from the RIS to the receiver,

This work was supported by the Villum Investigator Grant “WATER” from the Velux Foundation, Denmark. The work by P. Ramírez-Espinosa has been funded by the European Union under the Marie Skłodowska-Curie grant agreement No. 101109529.

R. J. Williams, O. Semenovska and P. Popovski are with Department of Electronic Systems, Connectivity Section, Aalborg University, 9220 Aalborg Øst, Denmark. E-mail: {rjw, ose, petarp}@es.aau.dk.

O. Semenovska is also with Electronic Engineering Department, National Technical University of Ukraine, Ukraine.

P. Ramírez-Espinosa is with Telecommunications Research Institute (TELMA), University of Málaga, 29071 Málaga, Spain. E-mail: pre@ic.uma.es.

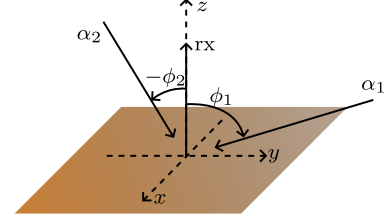


Fig. 1. Illustration of a RIS being illuminated by two planewaves. The impinging waves are scattered towards a user (rx) located in the broadside direction.

and Φ is a reflection matrix. In the simplest case, this reflection matrix is a diagonal matrix of unit amplitude entries, representing loss-less reflection of arbitrary phase. Due to its simplicity and the independence between Φ and the different channels, a plethora of works has dealt with channel estimation procedures, beamforming algorithms, RIS-based localization systems, and in general, problems where the target is optimizing the reflection matrix Φ with respect to any performance metric [3, 4].

Inheriting this simple cascaded channel, [5, 6] derived both the spatial correlation of \mathbf{H}_1 and \mathbf{H}_2 under Rayleigh fading and the channel matrices themselves in a line-of-sight deterministic channel based on an effective electrical aperture model of the RIS elements. A similar approach is used in [7], where each element has a radiation pattern and an aperture, being thus the power reflected by the element given by the product of the radiation pattern and the surface power density of the source field projected onto the aperture of the element. However, as proved in [8], the aperture of the reflecting element and its radiation pattern cannot be treated independently without violating power conservation. Central to all these works based on the cascaded channel is the fact that they rely on the strong assumption that the channel can be separated into three independent parts, i.e., \mathbf{H}_1 and \mathbf{H}_2 are completely independent of Φ . This assumption, though, has not been proven in general.

As an illustrative example of the present work, consider the scenario in Fig. 1 with a single electrically small RIS element that is illuminated by two plane waves with amplitudes α_1 and α_2 from two directions ϕ_1 and ϕ_2 . The element scatters the impinging waves towards a single receiver located in the $\phi_{\text{out}} = 0$ direction. The incoming and outgoing waves have the same polarization, and the element is constructed such that it acts as a reflector when illuminated from the direction $\phi = 0$. As we shall explain later on in Section IV, the RIS-assisted

channel is given as $h = C(g_1 + g_2)$ where

$$g_n = \alpha_n \left(e^{i\rho} (1 + \cos(\phi_n)) - i (1 - \cos(\phi_n)) \right) \quad (2)$$

and ρ is the phase-shift introduced by the element, with C and α_n some constants. From this simple example, we see that if and only if $\phi_n = 2m\pi$ for m a natural number, then $g_n = \alpha_n e^{i\rho}$ such that the channel admits the cascaded expression

$$h = \underbrace{C}_{h_1} \underbrace{e^{i\rho}}_{\Phi} \underbrace{(\alpha_1 + \alpha_2)}_{h_2}. \quad (3)$$

In other words, the cascaded channel is valid *only* for a single spatial direction.

Being aware of the limitations of the cascaded channel, more sophisticated models have been proposed, aiming to capture the electromagnetic phenomena inherent to RISs and rather neglected in the cascaded model. In [9], the RIS is modeled as an in-homogeneous impedance boundary subject to the physical optics approximation. The result is a model that is coherent with Maxwell's equations, and links the surface impedance to the reflection properties of the surface together with a set of conditions for power conservation. However, the model does not allow enforcing of power conservation on a microscopic scale, nor does it allow polarization transformations or breaking of reciprocity, as demonstrated using metasurface based designs [10, 11].

Approaches based on impedance models are presented in [12, 13], where the response of the RIS is no longer a linear term as in (1). They show, though, that this modified cascaded channel is valid if power conservation is ensured, although at the price of a significant reduction in the reflection phase-coverage. In fact, the elements phase-shift coverage is restricted to $\frac{\pi}{2}$ for a reflection coefficient amplitude of above 0.75, which is a consequence of considering a single electric dipole moment. Despite the limitations, the models are, nevertheless, useful to capture some physical limitations of RISs, and its application to communications have been studied in [14–16].

Scattering parameters-based formulations are given in [17, 18]. The former also assumes the off-diagonal entries of the reflection matrix Φ can take non-zero values. This is equivalent to a controllable mutual coupling, which would require complex and potentially active RIS designs. As is shown in [19], modeling of scattering is equivalent to modeling impedance parameters. By accounting for the fact that the total current flowing on the reflector is the superposition of both the current induced by the impinging wave and the currents reflected by an attached load, as opposed to only the reflected currents, the restricted phase-response remains. The work [20] brings further analytical details about the equivalence of scattering parameter, impedance parameter, and admittance parameter modeling, while [21] extends the modeling to a layered architecture of surfaces capable of spatial domain processing.

Despite the limitations shown in the previous works, it is known that metasurface based designs can provide full 2π phase-coverage in the reflection coefficient [11]. Additionally, new and exotic wave interactions such as polarization transformations and breaking of channel reciprocity have been demonstrated in [10, 22]. The purpose of this paper is to

introduce advances in metasurface modelling to the wireless community and thereby find potential applications and new research directions utilizing the exotic wave interactions enabled by metasurface based designs. Specifically, our contributions are

- We model the RIS as a collection of electrically small particles with dipolar response, including electric and magnetic moments, and characterized through their *polarizability* matrices. We clearly show the conditions under which these matrices represent *passive* and *reciprocal* RISs, both widely assumed properties.
- We demonstrate that the particles can be designed to modify phase, amplitude and polarization of the impinging wave, and detail the relationship between these magnitudes and the angular directions, proving that phase and amplitude are correlated, and showing when the cascaded channel becomes valid.
- The consequences of these findings in wireless communications are analyzed, questioning the standard channel estimation methods and characterizing the asymptotic behaviour of the RIS (large number of elements).
- We present a general framework to optimize the RIS aiming to maximize its utility in wireless, and show results where it is theoretically possible to improve the performance (e.g., phase coverage) compared to state-of-the-art models.

Paper overview: Sec. II starts with a short review of the prerequisite electromagnetic theory and presents the end-to-end channel model. Sec. III analysis the relationship between phase, amplitude, polarization and angular direction for passive and lossless RISs. Sec. IV analyzes the impact of such trade-off in common communications scenarios. Sec. V treats the optimization of the RIS configuration with respect to the received signal power. Sec. VI presents a range of simulation results and, finally, Sec. VII concludes the work and highlights main results.

Notation: i is the imaginary unit, $\|\cdot\|_2$ is the Euclidean norm, $|\cdot|$ is the absolute value, \cdot^T and \cdot^H are the transpose and Hermitian transpose respectively. Vectors are denoted by bold lowercase symbols, and matrices are denoted by bold uppercase symbols. $(\mathbf{A})_{n,m}$ denotes the element on the n 'th row and m 'th column of \mathbf{A} . $\text{Tr}\{\cdot\}$ is the trace operator and $\mathbb{E}[x]$ is the expectation operator. $\text{diag}(\mathbf{A})$ is a vector made the entries along the diagonal of \mathbf{A} and \odot is the Hadamard product. The shorthand notation $r = \|\mathbf{r}\|_2$ and $\hat{\mathbf{r}} = \mathbf{r}r^{-1}$ is used throughout the paper.

II. END-TO-END COMMUNICATIONS CHANNEL

We consider a narrowband RIS-assisted communication system consisting of one transmitter, one receiver, and one RIS, all suspended in a vacuum. Both the transmitter and the receiver are single antenna devices located at arbitrary positions $\mathbf{x}_t \in \mathbb{R}^{3 \times 1}$ and $\mathbf{x}_r \in \mathbb{R}^{3 \times 1}$. The RIS is modeled as a planar antenna structure centered at the origin of coordinates, and contained in the $z = 0$ plane (without any loss of generality). The RIS is made up of electrically small reconfigurable scattering structures, henceforth called particles, similarly as

how metasurfaces are constructed. Besides, we assume the thickness of the surface is negligible, following the envisioned idea of passive, cheap and thin RISs¹

As an electromagnetic wave from an external source—either the transmitter or any scatterer—hits the RIS, currents are induced in the particles. The particles scatter a so-called *interaction field* among them which in turn also induces new currents in the particles. This effect creates a dampened oscillation that continues until equilibrium, point at which the RIS carries statically oscillating electric and effective magnetic current distributions. Depending on these currents and the particle configuration, the impinging field is transmitted or reflected in a different way.

To establish the end-to-end communication channel between the transmitter and the user through both the direct and the RIS-assisted paths, we first review some fundamentals of electromagnetic radiation.

A. Electromagnetic radiation

Given some current distribution in space, represented by the electric $\mathbf{j} \in \mathbb{C}^{3 \times 1}$ and magnetic $\mathbf{m} \in \mathbb{C}^{3 \times 1}$ current vectors, the radiated electric $\mathbf{e} \in \mathbb{C}^{3 \times 1}$ and magnetic $\mathbf{h} \in \mathbb{C}^{3 \times 1}$ fields at an arbitrary point are given by [24, sec. 3.4]

$$\begin{bmatrix} \mathbf{e}(\mathbf{x} + \mathbf{x}) \\ \mathbf{h}(\mathbf{x} + \mathbf{x}) \end{bmatrix} = \iiint_{-\infty}^{\infty} \mathbf{G}(\mathbf{d} + \mathbf{x} - \bar{\mathbf{x}}) \begin{bmatrix} \mathbf{j}(\bar{\mathbf{x}} + \bar{\mathbf{x}}) \\ \mathbf{m}(\bar{\mathbf{x}} + \bar{\mathbf{x}}) \end{bmatrix} d\bar{\mathbf{x}}, \quad (4)$$

where $\mathbf{x} \in \mathbb{R}^{3 \times 1}$ and $\bar{\mathbf{x}} \in \mathbb{R}^{3 \times 1}$ point to the centers of the measurement and source volumes, $\mathbf{d} = \mathbf{x} - \bar{\mathbf{x}}$ is the distance vector from the source volume to the measurement volume, $\mathbf{x} \in \mathbb{R}^{3 \times 1}$ and $\bar{\mathbf{x}} \in \mathbb{R}^{3 \times 1}$ indicate a relative position w.r.t. \mathbf{x} and $\bar{\mathbf{x}}$, and $\mathbf{G}(\cdot) \in \mathbb{C}^{6 \times 6}$ is the free-space Green's function.

The Green's matrix is often written out in terms of the sub-matrices \mathbf{G}_{ee} , \mathbf{G}_{em} , \mathbf{G}_{me} , and \mathbf{G}_{mm} , denoting the electric-to-electric, magnetic-to-electric, electric-to-magnetic, and magnetic-to-magnetic spatial impulse-responses, respectively. Thus, we have

$$\mathbf{G}(\mathbf{r}) = ik \begin{bmatrix} \mathbf{G}_{ee}(\mathbf{r})\eta & \mathbf{G}_{em}(\mathbf{r}) \\ \mathbf{G}_{me}(\mathbf{r}) & \mathbf{G}_{mm}(\mathbf{r})\eta^{-1} \end{bmatrix}, \quad (5)$$

where $k = 2\pi/\lambda$ is the wavenumber, $\eta = \sqrt{\mu\epsilon^{-1}}$ is the free space impedance (μ and ϵ are the permeability and permittivity), and the distinct submatrices are given by

$$\mathbf{G}_{ee}(\mathbf{r}) = \mathbf{G}_{mm}(\mathbf{r}) = \frac{-1}{k^2} \left(k^2 \mathbf{I}_3 + \nabla \nabla^T \right) \frac{e^{-ikr}}{4\pi r}, \quad (6)$$

$$\mathbf{G}_{em}(\mathbf{r}) = -\mathbf{G}_{me}(\mathbf{r}) = \frac{-1}{ik} \left(\nabla \times \frac{e^{-ikr}}{4\pi r} \right). \quad (7)$$

If $\mathbf{r} \rightarrow \mathbf{0}$, then the following relation holds:

$$\mathbf{G}_0 = \lim_{\mathbf{r} \rightarrow \mathbf{0}_{3 \times 1}} \text{Re}\{\mathbf{G}(\mathbf{r})\} = \frac{-k^2}{6\pi} \begin{bmatrix} \mathbf{I}_3\eta & \mathbf{0}_{3 \times 3} \\ \mathbf{0}_{3 \times 3} & \mathbf{I}_3\eta^{-1} \end{bmatrix}. \quad (8)$$

¹The proposed modeling approach can, however, be easily extended to multiple layers of simple lattice structures, commonly referred to as stacked RISs [23].

In turn, in the far field (r is large) the higher order terms of the Green's matrices vanish, and they are approximated by

$$\begin{aligned} \mathbf{G}_{ee}^{\text{ff}}(\mathbf{d} + \mathbf{x} - \bar{\mathbf{x}}) &= \frac{e^{-ik(d + \hat{\mathbf{d}}^T(\mathbf{x} - \bar{\mathbf{x}}))}}{4\pi d} \mathbf{P}_1(\mathbf{d}), \\ \mathbf{G}_{em}^{\text{ff}}(\mathbf{d} + \mathbf{x} - \bar{\mathbf{x}}) &= \frac{e^{-ik(d + \hat{\mathbf{d}}^T(\mathbf{x} - \bar{\mathbf{x}}))}}{4\pi d} \mathbf{P}_2(\mathbf{d}), \\ \mathbf{P}_1(\mathbf{d}) &= d^{-2} \mathbf{d} \mathbf{d}^T - \mathbf{I}_3, \\ \mathbf{P}_2(\mathbf{d}) &= \frac{1}{d} \begin{bmatrix} 0 & -(\mathbf{d})_3 & (\mathbf{d})_2 \\ (\mathbf{d})_3 & 0 & -(\mathbf{d})_1 \\ -(\mathbf{d})_2 & (\mathbf{d})_1 & 0 \end{bmatrix}. \end{aligned} \quad (9)$$

Note that the far field assumption requires \mathbf{d} large and $\|\bar{\mathbf{x}}\|_2, \|\mathbf{x}\|_2 \ll d$. Inserting (9) into (4) yields the electromagnetic radiation in the far field as

$$\begin{bmatrix} \mathbf{e}(\mathbf{x} + \mathbf{x}) \\ \eta \mathbf{h}(\mathbf{x} + \mathbf{x}) \end{bmatrix} = \frac{e^{-ik(d + \hat{\mathbf{d}}^T \mathbf{x})}}{4\pi d} \begin{bmatrix} \mathbf{p} \\ \hat{\mathbf{d}} \times \mathbf{p} \end{bmatrix} \quad (10)$$

where

$$\mathbf{p} = ik \mathbf{P} \begin{bmatrix} \mathbf{I}_3\eta & \mathbf{0}_{3 \times 3} \\ \mathbf{0}_{3 \times 3} & \mathbf{I}_3 \end{bmatrix} \iiint_{\mathcal{V}_s} e^{ik\hat{\mathbf{d}}^T \bar{\mathbf{x}}} \begin{bmatrix} \mathbf{j}(\bar{\mathbf{x}}) \\ \mathbf{m}(\bar{\mathbf{x}}) \end{bmatrix} d\bar{\mathbf{x}}, \quad (11)$$

$$\mathbf{P} = [\mathbf{P}_1(\mathbf{d}) \quad \mathbf{P}_2(\mathbf{d})], \quad (12)$$

with \mathcal{V}_s the source volume. A closer look to (10) reveals that the field observed under far field conditions is described by a plane wave.

B. End-to-end channel and RIS radar cross section

As shown in (10), the far field wave always takes the shape of a plane wave, whether the wave originates directly from a transmit antenna, or is the result of scattering by the RIS. Hence we write the *planewave spectrum* of the field radiated by the transmitter as²

$$\mathbf{e}_t(\hat{\mathbf{r}}) = \frac{\eta}{\lambda} \mathbf{l}_t(\hat{\mathbf{r}}) s \quad (13)$$

where $s \in \mathbb{C}$ is a transmit symbol, $\hat{\mathbf{r}} \in \mathbb{R}^{3 \times 1}$ is a direction vector, and $\mathbf{l}_t(\hat{\mathbf{r}})$ is a power normalized effective length defined as

$$\mathbf{l}_t(\hat{\mathbf{r}}) = \frac{i}{2\sqrt{P_t}} \mathbf{P}(\hat{\mathbf{r}}) \iiint_{\mathcal{V}_t} e^{ik\hat{\mathbf{r}}^T \mathbf{x}_t} \begin{bmatrix} \mathbf{j}(\mathbf{x}_t) \\ \eta^{-1} \mathbf{m}(\mathbf{x}_t) \end{bmatrix} d\mathbf{x}_t, \quad (14)$$

where \mathcal{V}_t is the volume containing the transmitter current distribution, and $P_t \in \mathbb{R}^+$ is the reference transmitted power, i.e., the transmitted power when $\mathbb{E}[|s|^2] = 1$. From the plane wave spectrum in (13), the electric field at point \mathbf{x} in free space is directly given by $\mathbf{e}_t(\mathbf{x}) = \mathbf{e}_t \left(\frac{\mathbf{x} - \mathbf{x}_t}{\|\mathbf{x} - \mathbf{x}_t\|_2} \right) \frac{e^{-ik\|\mathbf{x} - \mathbf{x}_t\|_2}}{\|\mathbf{x} - \mathbf{x}_t\|_2}$.

As the wave in (13) propagates, it interacts with different scatterers in the environment, including the RIS. Thus, the wave impinges upon the received through two channels: the

²Note that we deliberately focus only on the electric field, as for a plane wave $\mathbf{h}(\mathbf{x}) = \eta^{-1} \hat{\mathbf{d}} \times \mathbf{e}(\mathbf{x})$.

direct channel \mathbf{h}_d and the RIS-assisted channel \mathbf{h}_a ; leading the planewave spectrum of the field at the receiver $\mathbf{e}_r(\hat{\mathbf{r}})$ given by

$$\mathbf{e}_r(\hat{\mathbf{r}}) = \frac{\eta}{\lambda} (\mathbf{h}_d(\hat{\mathbf{r}}) + \mathbf{h}_a(\hat{\mathbf{r}})) s, \quad (15)$$

$$\mathbf{h}_d(\hat{\mathbf{r}}) = \iint_{S_t} \mathbf{H}_{rt}(\hat{\mathbf{r}}, \hat{\mathbf{r}}_t) \mathbf{l}_t(\hat{\mathbf{r}}_t) d\hat{\mathbf{r}}_t, \quad (16)$$

$$\mathbf{h}_a(\hat{\mathbf{r}}) = \int \cdots \int_{S_{\text{out}}, S_{\text{in}}, S_t} \mathbf{H}_{rs}(\hat{\mathbf{r}}, \hat{\mathbf{r}}_{\text{out}}) \mathbf{S}(\hat{\mathbf{r}}_{\text{out}}, \hat{\mathbf{r}}_{\text{in}}) \mathbf{H}_{st}(\hat{\mathbf{r}}_{\text{in}}, \hat{\mathbf{r}}_t) \times \mathbf{l}_t(\hat{\mathbf{r}}_t) d\hat{\mathbf{r}}_t d\hat{\mathbf{r}}_{\text{in}} d\hat{\mathbf{r}}_{\text{out}}, \quad (17)$$

where $S_\xi \forall \xi \in \{r, t, \text{in}, \text{out}\}$ are unit-spheres and \mathbf{H}_{xy} is the double-directional channel [25, sec. 6.7] from actor y to x , encapsulating losses, polarization rotations and reflections (r denotes receiver, s is the RIS, and t is the transmitter). The scattering matrix \mathbf{S} in (17) captures the response of the RIS as a whole, describing how a impinging wave is transformed by the RIS in terms of amplitude, phase, and polarization. In other words, the planewave spectrum radiated by the RIS is described by

$$\mathbf{e}_s(\hat{\mathbf{r}}) = \mathbf{S}(\hat{\mathbf{r}}, \hat{\mathbf{r}}_{\text{in}}) \mathbf{e}_{\text{in}}(\hat{\mathbf{r}}_{\text{in}}), \quad (18)$$

where $\mathbf{e}_{\text{in}}(\hat{\mathbf{r}}_{\text{in}}) = \iint_{S_t} \mathbf{H}_{st}(\hat{\mathbf{r}}_{\text{in}}, \hat{\mathbf{r}}_t) \mathbf{l}_t(\hat{\mathbf{r}}_t) d\hat{\mathbf{r}}_t$ is the planewave spectrum of the ingoing electric field at the center of the RIS.

Assuming the receiver has a power normalized effective length \mathbf{l}_r , the received signal (with unit \sqrt{W}) is given by

$$\begin{aligned} v &= \frac{\eta}{2\lambda} \iint_{S_r} \mathbf{l}_r^H(-\hat{\mathbf{r}}_r) (\mathbf{h}_d(\hat{\mathbf{r}}_r) + \mathbf{h}_a(\hat{\mathbf{r}}_r)) s d\hat{\mathbf{r}}_r \\ &= \frac{\eta}{2\lambda} (h_d + h_a) s \end{aligned} \quad (19)$$

where the 2^{-1} factor accounts for the power-splitting between the antenna and a matched load ($\sqrt{2^{-1}}$) and the conversion from peak-values to time-averaged values ($\sqrt{2^{-1}}$). Note that (19) has the form of the conventional signal model assumed in communications, representing hence the end-to-end channel.

From (19), the channel gain is easily computed as

$$g = \frac{P_{\text{rx}}}{P_{\text{tx}}} = \frac{|v|^2}{|s|^2} = \left(\frac{\eta}{2\lambda} \right)^2 |h_d + h_a|^2 \quad (20)$$

and, in general, the objective is maximizing g by adjusting the configuration of the RIS, i.e. \mathbf{S} , to maximize the amplitude of h_a and align the phases of h_d and h_a to ensure coherent summation. To get further insight, we particularize for a line-of-sight channel; that is, a single plane wave. In this case, the channel matrices are described by

$$\mathbf{H}_{xy}(\hat{\mathbf{r}}_1, \hat{\mathbf{r}}_2) = \delta(\hat{\mathbf{r}}_1 - \hat{\mathbf{d}}_{xy}) \delta(\hat{\mathbf{r}}_2 - \hat{\mathbf{d}}_{xy}) \mathbf{I}_3 \frac{e^{-ikd_{xy}}}{d_{xy}}, \quad (21)$$

where $\mathbf{d}_{xy} = \mathbf{x}_x - \mathbf{x}_y$ is the distance vector from agent y to agent x . Therefore, the direct and RIS-assisted complex gains become

$$h_d = \frac{e^{-ikd_{rt}}}{d_{rt}} \mathbf{l}_r^H(-\hat{\mathbf{d}}_{rt}) \mathbf{l}_t(\hat{\mathbf{d}}_{rt}), \quad (22)$$

$$h_a = \frac{e^{-ik(d_{rs}+d_{st})}}{d_{rs}d_{st}} \mathbf{l}_r^H(-\hat{\mathbf{d}}_{rt}) \mathbf{S}(\hat{\mathbf{d}}_{rt}, \hat{\mathbf{d}}_{st}) \mathbf{l}_t(\hat{\mathbf{d}}_{st}), \quad (23)$$

and maximizing g becomes equivalent to maximizing

$$\begin{aligned} f &= |a_d \hat{\mathbf{l}}_r^H(-\hat{\mathbf{d}}_{rt}) \hat{\mathbf{l}}_t(\hat{\mathbf{d}}_{rt}) e^{-ikd_{rt}} \\ &\quad + a_a \hat{\mathbf{l}}_r^H(-\hat{\mathbf{d}}_{rs}) \hat{\mathbf{p}}_r(\hat{\mathbf{d}}_{rs}, \hat{\mathbf{d}}_{st}) e^{-ik(d_{rs}+d_{st})}|^2, \end{aligned} \quad (24)$$

where

$$a_d = d_{rt}^{-1} \sqrt{G_r(-\hat{\mathbf{d}}_{rt}) G_t(\hat{\mathbf{d}}_{rt})}, \quad (25)$$

$$a_a = d_{rs}^{-1} d_{st}^{-1} \sqrt{G_r(-\hat{\mathbf{d}}_{rs}) G_t(\hat{\mathbf{d}}_{st}) \frac{\bar{\sigma}}{4\pi}} \quad (26)$$

with $G_y = \frac{2\pi\eta_y^H \mathbf{l}_y}{\lambda^2}$ is the gain of the y 'th antenna, $\hat{\mathbf{p}}_r(\hat{\mathbf{d}}_{rs}, \hat{\mathbf{d}}_{st}) = \mathbf{S}(\hat{\mathbf{d}}_{rs}, \hat{\mathbf{d}}_{st}) \hat{\mathbf{l}}_t(\hat{\mathbf{d}}_{st}) \sqrt{\frac{4\pi}{\bar{\sigma}}}$, and

$$\bar{\sigma} = 4\pi \left\| \mathbf{S}(\hat{\mathbf{d}}_{rs}, \hat{\mathbf{d}}_{st}) \hat{\mathbf{l}}_t(\hat{\mathbf{d}}_{st}) \right\|_2^2 \quad (27)$$

is the the radar cross section (RCS) of the RIS.

With the goal of analyzing the wave manipulating capabilities of the RIS, we define the effective scattering, A_c , and the effective RCS, σ , of the RIS as

$$A_c = \hat{\mathbf{p}}_{\text{out}}^H \mathbf{S}(\hat{\mathbf{d}}_{rs}, \hat{\mathbf{d}}_{st}) \hat{\mathbf{p}}_{\text{in}}, \quad (28)$$

$$\sigma = |A_c|^2 4\pi, \quad (29)$$

where $\hat{\mathbf{p}}_{\text{in}}$ and $\hat{\mathbf{p}}_{\text{out}}$ are the polarization vectors of in- and out-going planewaves. Observe that setting

$$\hat{\mathbf{p}}_{\text{out}} = e^{-ik(d_{rt}-d_{st})} e^{i\angle(\hat{\mathbf{l}}_r^H(-\hat{\mathbf{d}}_{rt}) \hat{\mathbf{l}}_t(\hat{\mathbf{d}}_{rt}))} \hat{\mathbf{l}}_r(-\hat{\mathbf{d}}_{rs}), \quad (30)$$

$$\hat{\mathbf{p}}_{\text{in}} = e^{-ikd_{rs}} \hat{\mathbf{l}}_t(\hat{\mathbf{d}}_{st}) \quad (31)$$

and maximizing the utility of the RIS defined as

$$A = \text{Re}\{A_c\} = \text{Re}\left\{ \hat{\mathbf{p}}_{\text{out}}^H \mathbf{S}(\hat{\mathbf{d}}_{rs}, \hat{\mathbf{d}}_{st}) \hat{\mathbf{p}}_{\text{in}} \right\} \quad (32)$$

maximizes the degree to which the signal through the RIS-assisted path is phase-aligned with the signal through the direct path. As such, the utility A is a metric of degree to which the RIS is capable of producing polarization- and phase-rotations. In the specific case of independence between scattering amplitude and phase, maximization of the utility A is equivalent of maximizing the signal power. The utility A and (32) are used as the main optimization objective for the single-element analysis.

The remaining part of the modeling is thus to derive an expression for the scattering matrix $\mathbf{S}(\hat{\mathbf{r}}_{\text{out}}, \hat{\mathbf{r}}_{\text{in}})$.

C. RIS model and scattered field

The electromagnetic field scattered by the RIS can be computed by inserted its current distribution into (4)—or into (10) for far field radiation. However, the exact current distribution is a complicated function of the physical structure of the particles, being hence impractical. As the particles are electronically small, though, their scattering response is predominantly dipolar, and therefore we can replace them by a set of electric and effective magnetic dipole moments. This approximation allows us to *i)* assume the Green's matrices are

approximately constant over the volume of a single particle, and *ii*) calculate the scattered field as the sum of the contribution of each effective dipole. Then, (4) yields

$$\begin{aligned} \begin{bmatrix} \mathbf{e}_s(\mathbf{x} + \mathbf{x}) \\ \mathbf{h}_s(\mathbf{x} + \mathbf{x}) \end{bmatrix} &\approx \sum_{n=1}^N \begin{bmatrix} \mathbf{e}_n(\mathbf{x} + \mathbf{x}) \\ \mathbf{h}_n(\mathbf{x} + \mathbf{x}) \end{bmatrix} \\ &= \sum_{n=1}^N \mathbf{G}(\mathbf{x} + \mathbf{x} - \mathbf{x}_n) \begin{bmatrix} \mathbf{j}_n \\ \mathbf{m}_n \end{bmatrix}, \end{aligned} \quad (33)$$

where \mathbf{e}_s and \mathbf{h}_s are the fields scattered by the whole RIS, \mathbf{e}_n and \mathbf{h}_n are the fields scattered by the n -th particle, with N the total number of particle composing the RIS, and \mathbf{j}_n and \mathbf{m}_n are the currents carried by the n -th particle. Note that, with the dipolar approximation, \mathbf{j}_n and \mathbf{m}_n can be seen as the discretization of the current distributions \mathbf{j} and \mathbf{m} at the points \mathbf{x}_n (particles positions). It is important to also note that, as $\mathbf{G}(\cdot)$ is inversely proportional to the distance (c.f. (6)-(7)), the approximation of $\mathbf{G}(\cdot)$ being constant over the volume of the particle is only valid if that is significantly smaller than the inter-particle spacing when computing the interacting field between them.

Equation (33) provides the field scattered by the RIS in terms of the currents, so the next step is deriving the latter. When the RIS particles interact with an electromagnetic field, a current density is induced in them. These induced currents are commonly modelled as proportional to the *acting field* [11, 26–28], understanding by acting field not only the one impinging from the transmitter but also the fields generated by adjacent particles. Therefore, the field acting upon the i 'th particle— \mathbf{e}_{ai} and \mathbf{h}_{ai} —is as such given by

$$\begin{bmatrix} \mathbf{e}_{ai}(\mathbf{x}_i) \\ \mathbf{h}_{ai}(\mathbf{x}_i) \end{bmatrix} = \begin{bmatrix} \mathbf{e}_e(\mathbf{x}_i) \\ \mathbf{h}_e(\mathbf{x}_i) \end{bmatrix} + \sum_{n \neq i} \begin{bmatrix} \mathbf{e}_n(\mathbf{x}_i) \\ \mathbf{h}_n(\mathbf{x}_i) \end{bmatrix}, \quad (34)$$

where $\mathbf{e}_e, \mathbf{h}_e$ is the external field, i.e., that coming from the transmitter or any reflection in the environment. In line with (10), the external field is in general given as a distribution of plane waves under farfield conditions. With impinging planewave distribution $\mathbf{e}_{in}(\hat{\mathbf{r}}_{in})$, given as in (18), the external field is given as

$$\begin{bmatrix} \mathbf{e}_e(\mathbf{x}_i) \\ \mathbf{h}_e(\mathbf{x}_i) \end{bmatrix} = e^{-ik\hat{\mathbf{r}}_{in}^T \mathbf{x}_i} \begin{bmatrix} \mathbf{I}_3 & \mathbf{0}_{3 \times 3} \\ \mathbf{0}_{3 \times 3} & \mathbf{I}_3 \gamma^{-1} \end{bmatrix} \mathbf{O} \mathbf{e}_{in}(\hat{\mathbf{r}}_{in}) \quad (35)$$

$$\mathbf{O} = \begin{bmatrix} \mathbf{I}_3 & -\mathbf{P}_2(\hat{\mathbf{r}}_{in}) \end{bmatrix}^T. \quad (36)$$

With the external field characterized, let define a proportionality factor matrix $\mathbf{X} \in \mathbb{C}^{6 \times 6}$ such that the induced currents in the i -th particle are given by

$$\begin{bmatrix} \mathbf{j}_i \\ \mathbf{m}_i \end{bmatrix} = \mathbf{X}_i \begin{bmatrix} \mathbf{e}_{ai}(\mathbf{x}_i) \\ \mathbf{h}_{ai}(\mathbf{x}_i) \end{bmatrix}. \quad (37)$$

It is important to note that the factor \mathbf{X} is equivalent to the widely applied polarizability concept apart from a factor $i\omega$ [11, 26–28]. Thus, due to the similarity between them, we refer here to \mathbf{X} as the polarizability matrix. Recalling the dipolar particle response, \mathbf{X} characterizes the excitation of each magnetic and electric dipole moment due to the field strength at each direction, and depends on the specific particle

implementation and its configuration. Therefore, we assume \mathbf{X} is, in general, reconfigurable.

Remark 1 (Passive RIS). *Depending on the physical implementation of the RIS, different constraints apply to \mathbf{X} . An important one is that, to make the particles lossless and passive (being both a common assumption in wireless communications), then the condition*

$$\frac{\mathbf{X}_i + \mathbf{X}_i^H}{2} = -\mathbf{X}_i^H \mathbf{G}_0 \mathbf{X}_i \quad (38)$$

must hold (see Appendix A). Using the results in [29, Thm. 11], this translates into the structural constraint

$$\mathbf{X}_i = (-\mathbf{G}_0)^{-\frac{1}{2}} \frac{\mathbf{U}_i + \mathbf{I}_6}{2} (-\mathbf{G}_0)^{-\frac{1}{2}}, \quad (39)$$

where $\mathbf{U}_i \in \mathbb{C}^{6 \times 6}$ is any unitary matrix.

Considering that all the particles meet (39), the currents induced at the N particles can be obtained from (34)-(37), yielding a system of $6N$ equations and unknowns. Solving it and introducing the solution into (33), the planewave spectrum scattered by the RIS is obtained as

$$\begin{aligned} \mathbf{e}_s(\hat{\mathbf{r}}_{out}) &= \frac{i3}{4k} \mathbf{P} \mathbf{H} \left(\mathbf{I}_{6N} - \frac{i3\pi}{k} (\mathbf{V} + \mathbf{I}_{6N}) \mathbf{M} \right)^{-1} \\ &\quad \times (\mathbf{V} + \mathbf{I}_{6N}) \mathbf{T} \mathbf{O} \mathbf{e}_{in}(\hat{\mathbf{r}}_{in}), \end{aligned} \quad (40)$$

where the different involved matrices are defined as

$$\mathbf{H} = \begin{bmatrix} e^{ik\hat{\mathbf{r}}_{out}^T \mathbf{x}_1} \mathbf{I}_6 & e^{ik\hat{\mathbf{r}}_{out}^T \mathbf{x}_2} \mathbf{I}_6 & \dots & e^{ik\hat{\mathbf{r}}_{out}^T \mathbf{x}_N} \mathbf{I}_6 \end{bmatrix},$$

$$\mathbf{T} = \begin{bmatrix} e^{ik\hat{\mathbf{r}}_{in}^T \mathbf{x}_1} \mathbf{I}_6 & e^{ik\hat{\mathbf{r}}_{in}^T \mathbf{x}_2} \mathbf{I}_6 & \dots & e^{ik\hat{\mathbf{r}}_{in}^T \mathbf{x}_N} \mathbf{I}_6 \end{bmatrix}^H,$$

$$\mathbf{V} = \begin{bmatrix} \mathbf{U}_1 & 0 & \dots & 0 \\ 0 & \mathbf{U}_2 & \dots & 0 \\ \vdots & \vdots & \ddots & \vdots \\ 0 & 0 & \dots & \mathbf{U}_N \end{bmatrix},$$

$$\mathbf{M} = \begin{bmatrix} 0 & \mathbf{G}'(\mathbf{x}_1 - \mathbf{x}_2) & \dots & \mathbf{G}'(\mathbf{x}_1 - \mathbf{x}_N) \\ \mathbf{G}'(\mathbf{x}_2 - \mathbf{x}_1) & 0 & \dots & \mathbf{G}'(\mathbf{x}_2 - \mathbf{x}_N) \\ \vdots & \vdots & \ddots & \vdots \\ \mathbf{G}'(\mathbf{x}_N - \mathbf{x}_1) & \mathbf{G}'(\mathbf{x}_N - \mathbf{x}_2) & \dots & 0 \end{bmatrix},$$

$$\mathbf{G}'(\mathbf{x}) = \begin{bmatrix} \mathbf{G}_{ee}(\mathbf{x}) & \mathbf{G}_{em}(\mathbf{x}) \\ \mathbf{G}_{me}(\mathbf{x}) & \mathbf{G}_{mm}(\mathbf{x}) \end{bmatrix}.$$

Comparing (18) and (40) directly yields that the scattering matrix of the RIS is given as

$$\begin{aligned} \mathbf{S}(\hat{\mathbf{r}}_{out}, \hat{\mathbf{r}}_{in}) &= \frac{i3}{4k} \mathbf{P} \mathbf{H} \left(\mathbf{I}_{6N} - \frac{i3\pi}{k} (\mathbf{V} + \mathbf{I}_{6N}) \mathbf{M} \right)^{-1} \\ &\quad \times (\mathbf{V} + \mathbf{I}_{6N}) \mathbf{T} \mathbf{O}, \end{aligned} \quad (41)$$

completing the end-to-end channel modelling.

Remark 2 (Reciprocal RIS). *For many communication systems, and especially time-division-duplex multiple-input-multiple-output systems, channel reciprocity is exploited to significantly reduce system overhead. For RIS systems, channel reciprocity is not a given. Defining the submatrices of \mathbf{X}_i as*

$$\mathbf{X}_i = \begin{bmatrix} \mathbf{X}_{ee} & \mathbf{X}_{em} \\ \mathbf{X}_{me} & \mathbf{X}_{mm} \end{bmatrix}, \quad (42)$$

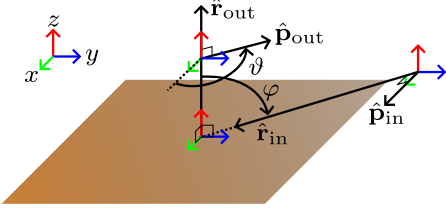


Fig. 2. Illustration of the geometry used in the single-element analysis.

then channel reciprocity holds if $\mathbf{X}_{ee} = \mathbf{X}_{ee}^T$, $\mathbf{X}_{mm} = \mathbf{X}_{mm}^T$, $\mathbf{X}_{em} = -\mathbf{X}_{me}^T$ (see Appendix A), which is always satisfied if \mathbf{X}_i is a diagonal matrix. Due to (39), identical symmetry constraints carries over to the four three-by-three submatrices of \mathbf{U}_i .

III. AMPLITUDE-PHASE RELATIONSHIP FOR PASSIVE AND LOSSLESS PARTICLES

A. RIS utility in terms of phase-shift, polarization and direction

The RIS scattering matrix \mathbf{S} can be reconfigured by modifying the particles polarizabilities in order to maximize the radiation towards a given direction or to change the polarization. To get insight in the relationship between arrival/departure directions, amplitude, phase and polarization of the outgoing wave, we first particularize (41) for a single particle³, yielding

$$\mathbf{S}(\hat{\mathbf{r}}_{\text{out}}, \hat{\mathbf{r}}_{\text{in}}) = \frac{i3}{4k} \mathbf{P} (\mathbf{U} + \mathbf{I}_6) \mathbf{O} \quad (43)$$

Introducing this into the utility function (32) leads to

$$\begin{aligned} A &= \frac{3}{4k} \text{Re} \left\{ i \hat{\mathbf{p}}_{\text{out}}^H \mathbf{P} (\mathbf{U} + \mathbf{I}_6) \mathbf{O} \hat{\mathbf{p}}_{\text{in}} \right\} \\ &= \frac{3}{4k} \text{Re} \left\{ \text{Tr} \left\{ \mathbf{U} \mathbf{U}' \Sigma \mathbf{V}^H \right\} + i \hat{\mathbf{p}}_{\text{out}}^H \mathbf{P} \mathbf{O} \hat{\mathbf{p}}_{\text{in}} \right\} \end{aligned}$$

where $\mathbf{U}' \Sigma \mathbf{V}^H = i \mathbf{O} \hat{\mathbf{p}}_{\text{in}} \hat{\mathbf{p}}_{\text{out}}^H \mathbf{P}$ is the singular value decomposition. Trivially, the utility $A = \text{Re}\{A_c\}$ is maximized when $\mathbf{U} = \mathbf{V} \mathbf{U}'^H$. The effective scattering, (28), under maximum utility is given as

$$A_c^* \stackrel{(a)}{=} \frac{3}{2k} + \frac{3i \hat{\mathbf{p}}_{\text{out}}^H \mathbf{P} \mathbf{O} \hat{\mathbf{p}}_{\text{in}}}{4k} \implies A^* = \text{Re}\{A_c^*\} \leq \frac{3}{k}, \quad (44)$$

where (a) uses the fact that, due to the structure of the problem, $(\Sigma)_{n,n} = 2$ for $n = 1$ and 0 otherwise. Note also that the solution $\mathbf{U} = \mathbf{V} \mathbf{U}'^H$ is not unique, and that it does not necessarily meet the conditions in Remark 2 (and hence the system may not be reciprocal).

As assumed in most of the works on RIS-assisted communications, one would expect maximum utility (i.e., $A = 3/k$) regardless the arrival/departure directions and the desired phase shift. However, we shall see that this is not met in practice. To further analyze this, we consider the case where the particle is excited by one plane wave with single polarization. Specifically, we assume direction of arrival and departure given by

$$\hat{\mathbf{r}}_{\text{in}} = [0 \quad -\sin(\varphi) \quad -\cos(\varphi)]^T, \quad \hat{\mathbf{r}}_{\text{out}} = [0 \quad 0 \quad 1]^T, \quad (45)$$

³This implies that $\mathbf{M} = \mathbf{0}$, $\mathbf{H} = \mathbf{T} = \mathbf{I}_6$.

and polarization vectors

$$\hat{\mathbf{p}}_{\text{in}} = [1 \quad 0 \quad 0]^T, \quad \hat{\mathbf{p}}_{\text{out}} = e^{i\rho} [\cos(\vartheta) \quad \sin(\vartheta) \quad 0]^T, \quad (46)$$

where $\rho \in [0, 2\pi)$ is the phase shift between the ingoing and outgoing waves. See Fig. 2 for a graphical illustration of the scenario.

In this scenario the effective scattering under maximum utility is given as

$$A_c^* = \frac{3}{2k} + \frac{3}{4k} i e^{-i\rho} \cos(\vartheta) (\cos(\varphi) - 1). \quad (47)$$

It is clearly observed that the scattering amplitude is a function of the spatial angles, the polarization rotation and the phase shift, invalidating the common assumption of independent amplitude and phase-shift. In fact, even for the case of parallel polarization, $\vartheta = 0$, the utility is maximized only for a relatively small subset of phase shifts and angular separations. Of special relevance are the two specific cases: *i*) orthogonal polarization— $\vartheta = \frac{\pi}{2}$, $\varphi \in [0, 2\pi)$, $\rho \in [0, 2\pi)$ —and *ii*) same angle— $\varphi = 0$, $\vartheta \in [0, 2\pi)$, $\rho \in [0, 2\pi)$ —where the maximum utility is independent of the phase-shift.

B. Constant amplitude phase-shifting under reciprocity constraint

Following with the previous case in (45)-(46), we aim to analyze now under which conditions it is correct to assume independence between amplitude and phase-shift. To that end, in the following we consider the effective scattering A_c particularized for parallel and orthogonal polarizations:

1) *Parallel polarization*, $\vartheta = 0$: In this case, from (43) and (45)-(46) we have

$$A_c|_{\vartheta=0} = \frac{3}{4k} e^{-i(\rho+\frac{\pi}{2})} \begin{bmatrix} -u_{1,5} - u_{5,5} - 1 \\ u_{1,6} + u_{5,6} \\ u_{1,1} + u_{5,1} + 1 \end{bmatrix}^T \begin{bmatrix} \cos(\varphi) \\ \sin(\varphi) \\ 1 \end{bmatrix}, \quad (48)$$

where $u_{m,n} = (\mathbf{U})_{m,n}$. Consider first the illustrative example of same direction of arrival/departure ($\varphi = 0$). In this scenario, we have

$$A_c|_{\varphi=0, \vartheta=0} = \frac{3e^{-i(\rho+\frac{\pi}{2})}}{4k} (u_{1,1} - u_{1,5} + u_{5,1} - u_{5,5}), \quad (49)$$

which, under the reciprocity constraints in Remark 2, attains its maximum value of $\frac{3}{2k}$ when either $u_{1,1} = -u_{5,5} = e^{i(\rho+\frac{\pi}{2})}$ and $u_{5,1} = u_{1,5} = 0$ (see (96) in Appendix B), or $u_{5,1} = -u_{1,5} = e^{i(\rho+\frac{\pi}{2})}$ and $u_{1,1} = u_{5,5} = 0$. In these cases $A_c|_{\varphi=0, \vartheta=0}$ is not a function of ρ and thus achieves constant amplitude phase-shifting. For angles $\varphi \neq 0$, the amplitude however varies with ρ . As an example, consider the case of orthogonal directions $\varphi = \pi/2$, which leads to

$$A_c|_{\varphi=\frac{\pi}{2}, \vartheta=0} = \frac{3e^{-i(\rho+\frac{\pi}{2})}}{4k} (1 + u_{1,1} + u_{1,6} + u_{5,1} + u_{5,6}) \quad (50)$$

where the real part can be maximized by setting $u_{1,1} = u_{5,6} = e^{i(\rho+\frac{\pi}{2})}$ and $u_{1,6} = u_{5,1} = 0$, yielding

$$A_c|_{\varphi=\frac{\pi}{2}, \vartheta=0} = \frac{3}{4k} \left(2 + e^{-i(\rho+\frac{\pi}{2})} \right) \quad (51)$$

which shows that the utility for a direction orthogonal to the impinging wave can be stronger than utility achieved for a direction parallel to the impinging wave. Maximum scattering is observed when the reflected wave is delayed by a quarter cycle, $\rho = -\frac{\pi}{2}$, and minimum scattering is observed for a phase-shift of $\rho = \frac{\pi}{2}$.

Interestingly, scattering amplitude can however be sacrificed to create constant amplitude phase-shifting, this is observed for the configuration \mathbf{U} given in (97) in Appendix B, for which $A_c|_{\varphi=\frac{\pi}{2},\vartheta=0} = 3/(4k)$, being independent of ρ .

Remark 3. From (48) we observe that, to achieve constant amplitude phase-shifting for every direction, the dependence on ρ and φ needs to be canceled out. This requires $u_{1,5} = -(u_{5,5} + 1)$, $u_{1,6} = -u_{5,6}$ and $u_{1,1} + u_{5,1} = \alpha e^{-i(\rho+\pi/2)} - 1$ with $\alpha \in \mathbb{R}$. Since \mathbf{U} is unitary for passive systems, hence $|u_{1,1}|^2 + |u_{5,1}|^2 \leq 1$, yielding $\alpha = 0$ as the only option, which implies no scattering. Therefore, it is not physically possible to achieve independence between phase and amplitude for parallel polarization.

2) *Orthogonal polarization, $\vartheta = \frac{\pi}{2}$:* In this case, we get

$$A_c|_{\vartheta=\frac{\pi}{2}} = \frac{3}{4k} e^{-i(\rho+\frac{\pi}{2})} \begin{bmatrix} u_{4,5} - u_{2,5} \\ u_{2,6} - u_{4,6} \\ u_{2,1} - u_{4,1} \end{bmatrix}^T \begin{bmatrix} \cos(\varphi) \\ \sin(\varphi) \\ 1 \end{bmatrix} \quad (52)$$

where it can be seen that constant amplitude phase-shifting is achieved for any one angle $\varphi = \phi$ by setting $u_{2,1} = e^{i(\rho+\frac{\pi}{2})}$, $u_{4,5} = \cos(\phi)e^{i(\rho+\frac{\pi}{2})}$, and $u_{4,6} = -\sin(\phi)e^{i(\rho+\frac{\pi}{2})}$ in which case $A_c|_{\vartheta=\frac{\pi}{2},\varphi=\phi} = 3/(2k)$. When an element is tuned for a single angle $\varphi = \phi$ in this manor, off-angle reflections, $\varphi \neq \phi$, does not provide constant amplitude phase-shifting. Finally, one can show that constant amplitude phase-shifting is possible for all on-axis directions simultaneously with the configuration given in (98) in Appendix B, yielding $A_c|_{\vartheta=\frac{\pi}{2}} = 3\sqrt{2}/(4k)$, which is completely independent of φ .

IV. IMPACT OF PHASE, AMPLITUDE AND ANGLE DEPENDENCY IN COMMUNICATIONS

A. Implications in cascaded channel model and channel estimation

In the following, we aim to evaluate the impact on wireless communications of the tight dependency between phase, amplitude, polarization and angle highlighted in the previous section. To that end, we analyze three different scenarios: *i*) a single particle in a line-of-sight channel, *ii*) a single particle in a random uniform planar scattering environment, known as Clarke's two-dimensional model [30, Sec. 5.4], and *iii*) a linear array of elements under Clarke's model.

1) *Single element, line-of-sight:* The RIS-assisted channel⁴ is given by (19) and (23) as

$$h = \frac{\eta}{2\lambda} \frac{e^{-ik(d_{rs}+d_{st})}}{d_{rs}d_{st}} \mathbf{I}_r^H(-\hat{\mathbf{d}}_{rs}) \mathbf{S}(\hat{\mathbf{d}}_{rs}, \hat{\mathbf{d}}_{st}) \mathbf{I}_t(\hat{\mathbf{d}}_{st}). \quad (53)$$

⁴The direct link between transmitter and receiver is here ignored.

With the transmitter and receiver located in the yz -plane at angles ϕ_1 and ϕ_2 w.r.t. the z -axis respectively, we have

$$\mathbf{I}_t(\hat{\mathbf{d}}_{st}) = a_t [1 \ 0 \ 0]^T, \quad \mathbf{I}_r(-\hat{\mathbf{d}}_{rs}) = a_r [1 \ 0 \ 0]^T, \quad (54)$$

$$\hat{\mathbf{d}}_{st} = \begin{bmatrix} 0 \\ -\sin(\phi_1) \\ -\cos(\phi_1) \end{bmatrix}, \quad \hat{\mathbf{d}}_{rs} = \begin{bmatrix} 0 \\ \sin(\phi_2) \\ \cos(\phi_2) \end{bmatrix},$$

with a_t and a_r as in (25) and (26). Consider also a parallel polarization as in (46) with $\vartheta = 0$. Introducing these into (53) and considering the scattering matrix (43), the resulting channel for a configuration \mathbf{U} for parallel directions (96), denoted by h_p , and for orthogonal directions (\mathbf{U} as in (97)), denoted by h_o , are given by

$$h_p(\rho) = \frac{3\eta}{16\pi} \frac{e^{-ik(d_{rs}+d_{st})}}{d_{rs}d_{st}} \left(g_{p1}e^{i\rho} - ig_{p2} \right) a_r a_t, \quad (55)$$

$$h_o(\rho) = \frac{3\eta}{16\pi} \frac{e^{-ik(d_{rs}+d_{st})}}{d_{rs}d_{st}} \left(e^{i\rho} - ig_o \right) a_r a_t, \quad (56)$$

where $g_{p1} = 1 + \cos(\phi_1)\cos(\phi_2)$, $g_{p2} = 1 - \cos(\phi_1)\cos(\phi_2)$ and $g_o = 1 - (\sin(\phi_1) + \cos(\phi_1))(\sin(\phi_2) + \cos(\phi_2))$. Interestingly, observe that, for two different phase-shifts ρ_1 and ρ_2 , the following holds:

$$h_p(\rho_1) = h_p(\rho_2) \frac{g_{p1}e^{i\rho_1} - ig_{p2}}{g_{p1}e^{i\rho_2} - ig_{p2}}, \quad (57)$$

$$h_o(\rho_1) = h_o(\rho_2) \frac{e^{i\rho_1} - ig_o}{e^{i\rho_2} - ig_o}. \quad (58)$$

The above relation has a strong implication in wireless communications. Usually, to estimate the end-to-end channel (RIS-assisted path), the RIS is fixed to a certain configuration—i.e., a certain ρ , and the cascaded channel is then estimated, assuming this estimation of the transmitter-to-RIS and RIS-to-receiver channels remains valid for others phase-shifts. However, looking at (57)-(58), we see that predicting $h(\rho_1)$ based on $h(\rho_2)$ requires not only information about $h(\rho_2)$ itself, but also knowledge about the angular positions of the transmitter and receiver (equivalently, $g_{p,1}$, $g_{p,2}$ and g_o). In effect, this means that even for a single element RIS, multiple pilot symbols are necessary to fully know the channel due to the lack of constant amplitude phase-shifting for all angles simultaneously.

Assume now an orthogonal polarization ($\vartheta = \pi/2$ in (46)), and a configuration matrix \mathbf{U} as in (98). Setting $\mathbf{I}_r(-\hat{\mathbf{d}}_{rs}) = a_r [0 \ 1 \ 0]^T$ yields a received signal

$$h_r(\rho) = \frac{3\eta\sqrt{2}}{32\pi} \cos(\phi_2) (1 + \cos(\phi_2)) e^{i\rho} a_r a_t, \quad (59)$$

where there is no dependence on the angular direction due to the constant amplitude phase-shifting achieved for orthogonal polarizations (c.f. Section III-B2). Then, for two different phase-shifts ρ_1 and ρ_2 , we get now

$$h_r(\rho_1) = v_r(\rho_2) e^{i(\rho_1-\rho_2)}, \quad (60)$$

which implies that one only needs knowledge of $v_r(\rho_2)$ to fully know the channel for any phase-shift ρ . In contrary to the parallel polarization case, full channel information across different reflection phases can be achieved by sending only a single known pilot symbol.

2) *Single element, multiple paths*: To analyze this case, we follow the same steps as before, but assuming now that the transmitter-to-RIS channel is no longer line-of-sight but describer according to Clarke's model. Hence, the wave impinging upon the RIS is a sum of M , x -polarized plane waves, all travelling in the yz -plane, i.e.,

$$\mathbf{H}_{\text{st}}(\hat{\mathbf{r}}, \hat{\mathbf{r}}_t) \mathbf{l}_t(\hat{\mathbf{r}}_t) = \sum_{n=0}^M [\alpha_n \ 0 \ 0]^\top \delta(\hat{\mathbf{r}}_t - \hat{\mathbf{r}}_n), \quad (61)$$

where $\alpha_n \in \mathbb{C}$ is a set of circularly symmetric i.i.d. random variables, and $\hat{\mathbf{r}}_n = [0 \ -\sin(\phi_n) \ -\cos(\phi_n)]^\top$ with $\phi_n \sim \mathcal{U}(0, 2\pi)$. From (17) and (19), the RIS-assisted channel is thus given by

$$h = \frac{\eta}{2\lambda} \frac{e^{-ikd_{\text{rs}}}}{d_{\text{rs}}} \mathbf{l}_r^\text{H}(-\hat{\mathbf{d}}_{\text{rs}}) \sum_{n=0}^M \mathbf{S}(\hat{\mathbf{d}}_{\text{rs}}, \hat{\mathbf{r}}_n) \begin{bmatrix} \alpha_n \\ 0 \\ 0 \end{bmatrix} \delta(\hat{\mathbf{r}}_t - \hat{\mathbf{r}}_n). \quad (62)$$

Particularizing for $\hat{\mathbf{d}}_{\text{rs}} = [0 \ 0 \ 1]^\top$ and considering parallel polarization, the end-to-end channel for parallel and orthogonal configurations in (96) and (97), respectively, yields

$$h_{\text{p}}(\rho) = \frac{3\eta}{16\pi} \frac{e^{-ikd_{\text{rs}}}}{d_{\text{rs}}} a_{\text{r}} \sum_{n=0}^M (g_{\text{p}1,n} e^{i\rho} - i g_{\text{p}2,n}) \alpha_n, \quad (63)$$

$$h_{\text{o}}(\rho) = \frac{3\eta}{16\pi} \frac{e^{-ikd_{\text{rs}}}}{d_{\text{rs}}} a_{\text{r}} \sum_{n=0}^M (e^{i\rho} - i g_{\text{o},n}) \alpha_n, \quad (64)$$

with $g_{\text{p}1,n} = 1 + \cos(\phi_n)$, $g_{\text{p}2,n} = 1 - \cos(\phi_n)$ and $g_{\text{o},n} = 1 - (\sin(\phi_n) + \cos(\phi_n))$.

As $M \rightarrow \infty$, as stated in Clarke's model, the central limit theorem holds and $h_m \sim \mathcal{CN}(0, \Sigma_m(\rho)^2)$ with $m = \{\text{p}, \text{o}\}$ and

$$\Sigma_{\text{p}}^2(\rho_1, \rho_2) = \mathbb{E}[h_{\text{p}}(\rho_1) h_{\text{p}}^*(\rho_2)] \quad (65)$$

$$= \left(\frac{3\eta |a_{\text{r}}| \Sigma_a}{16\pi d_{\text{rs}}} \right)^2 \frac{i(e^{i\rho_1} - e^{-i\rho_2}) + 3(1 + e^{i(\rho_1 - \rho_2)})}{2},$$

$$\Sigma_{\text{o}}^2(\rho_1, \rho_2) = \mathbb{E}[h_{\text{o}}(\rho_1) h_{\text{o}}^*(\rho_2)] \quad (66)$$

$$= \left(\frac{3\eta |a_{\text{r}}| \Sigma_a}{16\pi d_{\text{rs}}} \right)^2 \left(i(e^{i\rho_1} + e^{-i\rho_2}) + e^{i(\rho_1 - \rho_2)} + 2 \right),$$

where $\Sigma_a^2 = N \mathbb{E}[|\alpha_n|^2]$. In effect, the signal is a joint Gaussian distribution across different phase-shifts, given that polarization is preserved. This in turn means that when considering the cascaded channel (1) as

$$h = h_{\text{rs}} \varphi h_{\text{st}} \quad |\varphi| \leq 1, \quad (67)$$

one cannot assume that h_{st} and h_{rs} remains constant across different φ . In fact, as is shown here, h_{st} and h_{rs} are correlated random variables across different phase-shifts, φ . As anticipated, the randomness of the channel across different phase-shifts has big consequences for signal space channel estimation procedures. This will be further explored next.

3) *Multiple elements, multiple paths*: Let us generalize the previous scenario to a complete RIS made from N particles, and consider for analytical simplicity in this example that the elements are sufficiently spaced so that spatial correlation and inter-element coupling is negligible. Then, the received signal in the m -th symbol period is the contribution of the N independent elements as

$$q_m = \sum_{n=1}^N h_n(\rho_{n,m}) \quad (68)$$

where $\rho_{n,m}$ is the phase-shift applied by the n -th RIS element in the m -th symbol period.

Assuming we have M periods, we can write the theoretical received signal vector $\tilde{\mathbf{q}}$ predicted by the cascaded channel model as

$$\tilde{\mathbf{q}} = \mathcal{P} \mathbf{h}, \quad (69)$$

where $(\mathcal{P})_{n,m} = e^{i\rho_{n,m}}$ is the phase-shifting matrix of the RIS and, as the cascaded model assumes that the ingoing and outgoing channels are independent, $(\mathbf{h})_n = h_n(0)$. Note that we assume the channel remains constant for $m = 1, \dots, M$. From (69), one can draw the conclusion that given $N = M$ and \mathcal{P} being full rank, the channel \mathbf{h} can be estimated as

$$\tilde{\mathbf{h}} = \mathcal{P}^{-1} \tilde{\mathbf{q}}. \quad (70)$$

The optimal set of phase-shifts ρ_n^* is thus the set of phases which cancels the phase of $(\tilde{\mathbf{h}})_n$ such that the product $(\tilde{\mathbf{h}})_n e^{i\rho_n^*} = \left| (\tilde{\mathbf{h}})_n \right|$. We can define therefore the metric γ as the power ratio of the actual signal power versus the expected signal power according to the cascaded channel, i.e.,

$$\gamma = \left(\frac{\left| \sum_{n=1}^N h_n(\rho_n^*) \right|^2}{\sum_{n=1}^N \left| (\tilde{\mathbf{h}})_n \right|^2} \right). \quad (71)$$

This metric is evaluated numerically, and its empirical cumulative distribution function is plotted in Fig. 3 for different RIS sizes, where \mathcal{P} is the discrete Fourier transform matrix, and two configurations—parallel (96) and orthogonal (97) reflections—are employed (97). It is interesting that, as N grows, the variance in both configurations gets smaller while $\mathbb{E}[\gamma] \rightarrow 1$. Hence, for a sufficiently large array, the estimated signal power tends to the actual signal power.

Another metric of interest is the power loss ξ , defined as

$$\xi = \left(\frac{\left| \sum_{n=1}^N h_n(\rho_n^*) \right|^2}{\left| \sum_{n=1}^N (\mathbf{h}^*)_n \right|^2} \right) \quad (72)$$

where \mathbf{h}^* is the signal vector given an optimal configuration which maximizes the received signal power and ρ_n^* is again chosen assuming the validity of cascaded channel. Thus, ξ measures how much power is lost when configuring the RIS based on the cascaded channel estimation. This metric is evaluated in Fig. 4, which shows its empirical cumulative distribution functions, computed using the same \mathcal{P} and element

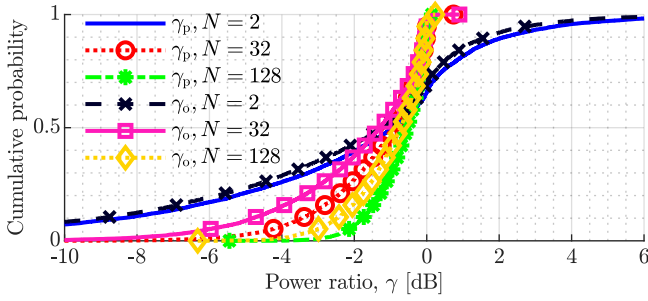


Fig. 3. An empirical cumulative distribution function based on Monte Carlo simulations of the power ratio γ (71) for the two element configurations; Parallel reflection γ_p , and Orthogonal reflection γ_o .

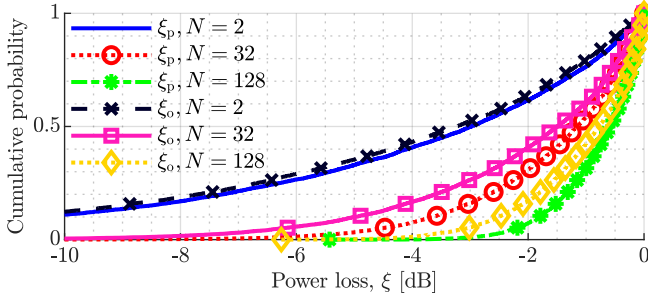


Fig. 4. An empirical cumulative distribution function based on Monte Carlo simulations of the power loss ξ (72) for the two element configurations; Parallel reflection ξ_p , and Orthogonal reflection ξ_o .

configurations as before. The channel \mathbf{h}^* is obtained by doing a grid search over $\nu = [-\pi; \pi]$ where the phase shift of the n 'th element is $\rho_n = \nu - \angle k_n$, with

$$k_{pn} = \sum_{m=0}^{\infty} \left(1 + \cos(\phi_{n,m})\right) \alpha_{n,m}, \quad k_{on} = \sum_{m=0}^{\infty} \alpha_{n,m}$$

for the parallel and orthogonal configurations, respectively.

From Fig. 4, we see again that as more elements are added to the RIS, the configuration obtained through the (cascaded channel) estimation procedure converges to the optimal one with an increasing probability. In fact, when $N = 128$, the median power loss due to suboptimal configuration is only -0.58 dB.

Remark 4. *In general, the cascaded channel in (1) is violated, as the transmitter-to-RIS and RIS-to-receiver channels are not independent but inherently correlated and dependent on applied phase-shift. Hence, multiple pilots are required to estimate the end-to-end channel even in the simplest case of a single element. As the number of elements grows, the conventional channel estimation scheme becomes more valid, and the resulting RIS configuration converges in the limit to the optimal one.*

B. One-way communication

We turn our attention now to the impact of the dependence between amplitude, phase and polarization in achieving one-way communications. Thus, consider again a single particle in isolation, with transmitter and receiver as in (45) and polarizations as in (46). Denote by A_d and A_u the downlink

(from transmitter to receiver) and uplink (from receiver to transmitter) complex responses. Then, analogously as in Section III-B, for parallel polarization ($\vartheta = 0$) we have

$$A_d = \frac{3}{4k} e^{-i(\rho + \frac{\pi}{2})} \begin{bmatrix} -u_{1,5} - u_{5,5} - 1 \\ u_{1,6} + u_{5,6} \\ u_{1,1} + u_{5,1} + 1 \end{bmatrix}^T \begin{bmatrix} \cos(\varphi) \\ \sin(\varphi) \\ 1 \end{bmatrix}, \quad (73)$$

$$A_u = \frac{3}{4k} e^{-i(\rho + \frac{\pi}{2})} \begin{bmatrix} u_{5,1} - u_{5,5} - 1 \\ -u_{6,1} + u_{6,5} \\ u_{1,1} - u_{1,5} + 1 \end{bmatrix}^T \begin{bmatrix} \cos(\varphi) \\ \sin(\varphi) \\ 1 \end{bmatrix}. \quad (74)$$

We see that, if $\varphi = 0$, i.e. transmitter and receiver are in the same angular direction, then $A_d = A_u$, and one-way communication is not possible; result that, up to some point, was expected. If, in turn, we particularize for orthogonal angular directions ($\varphi = \frac{\pi}{2}$), then

$$A_d = \frac{3}{4k} e^{-i(\rho + \frac{\pi}{2})} (1 + u_{1,1} + u_{1,6} + u_{5,1} + u_{5,6}), \quad (75)$$

$$A_u = \frac{3}{4k} e^{-i(\rho + \frac{\pi}{2})} (1 + u_{1,1} - u_{6,1} - u_{1,5} + u_{6,5}). \quad (76)$$

Setting $u_{1,1} = -1$, $u_{5,6} = e^{i(\rho + \frac{\pi}{2})}$, and $u_{1,6} = u_{5,1} = u_{6,1} = u_{1,5} = u_{6,5} = 0$ yields $A_u = 0$ and $A_d = 3/(4k)$, which proves that it is possible to do one-way communication under power conservation if the transmitter and receiver directions are orthogonal and polarizations are parallel.

Similarly, for orthogonal polarizations ($\vartheta = \frac{\pi}{2}$),

$$A_d = \frac{3}{4k} e^{-i(\rho + \frac{\pi}{2})} \begin{bmatrix} u_{4,5} - u_{2,5} \\ u_{2,6} - u_{4,6} \\ u_{2,1} - u_{4,1} \end{bmatrix}^T \begin{bmatrix} \cos(\varphi) \\ \sin(\varphi) \\ 1 \end{bmatrix}, \quad (77)$$

$$A_u = \frac{3}{4k} e^{-i(\rho + \frac{\pi}{2})} \begin{bmatrix} u_{5,4} + u_{5,2} \\ -u_{6,2} - u_{6,4} \\ u_{1,2} + u_{1,4} \end{bmatrix}^T \begin{bmatrix} \cos(\varphi) \\ \sin(\varphi) \\ 1 \end{bmatrix}.$$

Setting $u_{5,4} = -u_{5,2}$, $u_{6,4} = -u_{6,2}$, $u_{1,4} = -u_{1,2}$, $u_{2,1} = e^{i(\rho + \frac{\pi}{2})}$, $u_{4,5} = \cos(\varphi) e^{i(\rho + \frac{\pi}{2})}$, and $u_{4,6} = -\sin(\varphi) e^{i(\rho + \frac{\pi}{2})}$, one obtains that $A_d = 3/(2k)$ and $A_u = 0$, regardless of the angular separation φ . This implies that if the polarizations are orthogonal, one-way communications is possible for any single separation angle φ . In fact, it is possible to have one-way communication from all on-axis angles simultaneously, as is observed for the case configuration in (99) in Appendix B, in which case

$$A_d = \frac{3}{2k} \frac{1}{\sqrt{2}}, \quad A_u = 0, \quad (78)$$

for all separation angles, φ , simultaneously.

C. Spatial multiplexing

Finally, this section demonstrates that a RIS can support multiple orthogonal channels while meeting the reciprocity and power conservation conditions in Remarks 1 and 2. To this end, assume two transmitters and two receivers (all linearly polarized along x) located in the z -positive part of the yz -plane. As the RIS is in the xy -plane, this scenario is equivalent of a network with receivers and transmitters separated in the horizontal dimensions, as is usually the case for terrestrial

networks. It is important to note that, although we focus here on proving the case of two orthogonal channels, additional channels can be supported by using different polarizations and positions off yz -plane. Consider then the following directions and polarizations

$$\begin{aligned} \hat{\mathbf{p}}_{\text{in},t} &= [1 \ 0 \ 0]^\top, & \hat{\mathbf{p}}_{\text{out},t} &= [1 \ 0 \ 0]^\top, \\ \hat{\mathbf{r}}_{\text{in},t} &= \begin{bmatrix} 0 \\ -\sin(\varphi_t) \\ -\cos(\varphi_t) \end{bmatrix}, & \hat{\mathbf{r}}_{\text{out},t} &= \begin{bmatrix} 0 \\ \sin(\varphi_t - \Delta_t) \\ \cos(\varphi_t - \Delta_t) \end{bmatrix}. \end{aligned} \quad (79)$$

where $t = \{1, 2\}$ refer to the first and second end-to-end channels, i.e., the first or second pair of transmitter-receiver we aim to multiplex. Therefore, the effective scattering function between channels t and s is given by (28) as

$$A_{ts} = \hat{\mathbf{p}}_{\text{out},t}^H \mathbf{S}(\hat{\mathbf{r}}_{\text{out},t}, \hat{\mathbf{r}}_{\text{in},s}) \hat{\mathbf{p}}_{\text{in},s} \quad (80)$$

with $t, s = \{1, 2\}$. To achieve mutiplexing, we require the RIS to cancel the inter-channel interference while maximizing the scattering through the intended user. Mathematically, we need thus that $A_{12} = A_{21} = 0$ while maximizing A_{11} and A_{22} . Two examples meeting these constraints are given next, where for simplicity a single RIS element is considered:

1) $\varphi_1 = -\varphi_2 = \frac{\pi}{4}$, $\Delta_1 = \Delta_2 = 0$: Here, it can be proved that orthogonality is achieved for $u_{6,6} = 2\sqrt{2}u_{1,5} - 2u_{1,1} + u_{5,5} - 2$, while setting $u_{1,1} = -1$ and $u_{1,5} = 0$ ensures that power is conserved and $u_{5,5} = -e^{i\frac{\pi}{2}}$ maximizes the scattering of the signals under the previous conditions. The full matrix is given in (100) in Appendix B. For this particle configuration, we get $A_{11} = A_{22} = 3(1+i)/(4k)$ and $A_{11} = A_{22} = 0$.

2) $\varphi_1 = -\varphi_2 = \frac{\pi}{6}$, $\Delta_1 = \Delta_2 = \frac{\pi}{2}$: In this case, orthogonality require $u_{5,6} = -\frac{(1+\sqrt{3})}{2}u_{1,6}$ and

$$u_{1,1} = \frac{1}{4} \left((2u_{1,5} + u_{5,5} + u_{6,6} + 2) \sqrt{3} + 2u_{1,5} - 4 \right). \quad (81)$$

Under these conditions, the scattering of the desired signal is maximized if $u_{6,6} = 1$. An example of an unitary matrix meeting the previous conditions is given in (101), yielding $A_{21} = A_{12} = 0$ and

$$A_{11} = A_{22} = \frac{-i3\sqrt{3}}{4k}. \quad (82)$$

V. MAXIMIZING RIS RADAR CROSS SECTION

This section treats optimization of the effective RCS $\sigma = 4\pi |\hat{\mathbf{p}}_{\text{out}}^H \mathbf{S}(\hat{\mathbf{r}}_{\text{out}}, \hat{\mathbf{r}}_{\text{in}}) \hat{\mathbf{p}}_{\text{in}}|^2$ in (29) given known ingoing and outgoing wave normals and polarizations $\hat{\mathbf{r}}_{\text{in}}$, $\hat{\mathbf{p}}_{\text{in}}$, $\hat{\mathbf{r}}_{\text{out}}$, and $\hat{\mathbf{p}}_{\text{out}}$. That is, we aim to maximize the RIS utility in a generic communications problem, leading to the formulation:

$$\begin{aligned} \underset{\mathbf{V}}{\text{maximize}} \quad & f(\mathbf{V}) = \left| \hat{\mathbf{p}}_{\text{out}}^H \mathbf{S}(\hat{\mathbf{r}}_{\text{out}}, \hat{\mathbf{r}}_{\text{in}}) \hat{\mathbf{p}}_{\text{in}} \right|^2 \\ \text{subject to} \quad & \mathbf{V}^H \mathbf{V} = \mathbf{V} \mathbf{V}^H = \mathbf{I}_{6N}, \end{aligned} \quad (83)$$

where \mathbf{S} is given in (41) and \mathbf{V} is a block diagonal matrix of unitary matrices as defined in (41). Solutions to (83) are obtained through the following two methods:

- 1) Numeric optimization over Riemannian manifold.
- 2) Closed form solution in absence of interaction field.

A. Numeric optimization over Riemannian manifold

In the general case, \mathbf{V} is a block-diagonal unitary matrix, which implies each of the blocks themselves are unitary matrices, i.e., $\mathbf{U}_n^H \mathbf{U}_n = \mathbf{U}_n \mathbf{U}_n^H = \mathbf{I}_6 \ \forall n$. Due to the unitary constraint, a practical approach is optimizing directly on the unitary matrix group, similarly to [31]. Specifically, the `manopt` library is employed [32]. The Euclidean gradient is easily computed by applying standard techniques (the reader is gently referred to [33] for basic theory on complex-valued matrix derivatives), yielding

$$\frac{\partial f(\mathbf{V})}{\partial \mathbf{V}^*} = S \left(\mathbf{D}^H - \frac{3i\pi}{k} \mathbf{D}^H (\mathbf{V} + \mathbf{I}_{6N})^H \mathbf{E}^H \mathbf{M}^H \right), \quad (84)$$

where

$$\begin{aligned} \mathbf{D} &= \left(\frac{3}{4k} \right)^2 \mathbf{TO} \hat{\mathbf{p}}_{\text{in}} \hat{\mathbf{p}}_{\text{in}}^H \mathbf{O}^H \mathbf{T}^H (\mathbf{V} + \mathbf{I}_{6N})^H \times \\ &\quad \mathbf{E}^H \mathbf{H}^H \mathbf{P}^H \hat{\mathbf{p}}_{\text{out}} \hat{\mathbf{p}}_{\text{out}}^H \mathbf{P} \mathbf{E}, \\ \mathbf{E} &= \left[\mathbf{I}_{6N} - \frac{i3\pi}{k} (\mathbf{V} + \mathbf{I}_{6N}) \mathbf{M} \right]^{-1}, \end{aligned}$$

and $S(\cdot)$ selects the block diagonal blocks according to (41). Numerical optimization through the `manopt` library using the `unitaryfactory` manifold yields a local maximum of the objective function that approximately satisfies the constraint. A suboptimal solution satisfying the reciprocity constraints can be obtained by setting $S(\mathbf{V}) = \mathbf{V} \odot \mathbf{I}_{6N}$, restricting \mathbf{V} to be a diagonal matrix. The closed form solution given in sec. V-B is used as the initial point for the optimization.

B. Closed form solution in absence of interaction field

Due to the dependency between amplitude and phase of the scattered wave, see (47), maximization of the RCS requires joint optimization of all particles even in the absence of the interaction field. Under the assumption of independence between scattering amplitude and phase, the particles can be optimized in isolation and a closed form solution can be obtained. Assuming independence between scattering amplitude and phase, solving (83) is equivalent to solving

$$\begin{aligned} \underset{\mathbf{V}}{\text{maximize}} \quad & A = \text{Re} \left\{ \hat{\mathbf{p}}_{\text{out}}^H \mathbf{S}(\hat{\mathbf{r}}_{\text{out}}, \hat{\mathbf{r}}_{\text{in}}) \hat{\mathbf{p}}_{\text{in}} \right\}, \\ \text{subject to} \quad & \mathbf{V}^H \mathbf{V} = \mathbf{V} \mathbf{V}^H = \mathbf{I}_{6N}. \end{aligned} \quad (85)$$

Given no interaction field, equivalent to setting $\mathbf{M} = \mathbf{0}_{6N \times 6N}$, (85) is equivalent to

$$\begin{aligned} \underset{\mathbf{V}}{\text{maximize}} \quad & f(\mathbf{V}) = \text{Re} \left\{ \text{Tr} \left\{ i \mathbf{TO} \hat{\mathbf{p}}_{\text{in}} \hat{\mathbf{p}}_{\text{out}}^H \mathbf{P} \mathbf{H} \mathbf{V} \right\} \right\} \\ \text{subject to} \quad & \mathbf{V}^H \mathbf{V} = \mathbf{V} \mathbf{V}^H = \mathbf{I}_{6N}. \end{aligned} \quad (86)$$

As \mathbf{V} is block diagonal matrix of matrices \mathbf{U}_n , the objective function $f(\mathbf{V})$ can be rewritten as

$$f(\mathbf{V}) = \sum_{n=1}^N \text{Re} \left\{ \text{Tr} \{ \mathbf{A}_n \mathbf{U}_n \} \right\} \quad (87)$$

where $\mathbf{A}_n = i \mathbf{O} \hat{\mathbf{p}}_{\text{in}} \hat{\mathbf{p}}_{\text{out}}^H \mathbf{P} e^{-ik(\hat{\mathbf{r}}_{\text{in}} - \hat{\mathbf{r}}_{\text{out}})^T \bar{\mathbf{x}}_n}$ and $\bar{\mathbf{x}}_n$ is the relative position of the n 'th RIS particle. Similarly to what is done in (44), the objective function (87) is maximized by computing

the singular value decomposition of $\mathbf{A}_n = \mathbf{Y}_n \mathbf{\Sigma} \mathbf{K}_n^H$ and setting $\mathbf{U}_n = \mathbf{K}_n \mathbf{Y}_n^H$. The solution is therefore given as

$$\mathbf{V} = \begin{bmatrix} \mathbf{K}_1 \mathbf{Y}_1^H & 0 & \cdots & 0 \\ 0 & \mathbf{K}_2 \mathbf{Y}_2^H & \cdots & 0 \\ \vdots & \vdots & \ddots & \vdots \\ 0 & 0 & \cdots & \mathbf{K}_N \mathbf{Y}_N^H \end{bmatrix}. \quad (88)$$

Restricting \mathbf{V} to be a diagonal matrix yields

$$\mathbf{V} = e^{-\angle(i\text{TO}\hat{\mathbf{p}}_{\text{in}}\hat{\mathbf{p}}_{\text{out}}^H\mathbf{P}\mathbf{H})} \odot \mathbf{I}_{6N}. \quad (89)$$

where $e^{(\cdot)}$ is the element-wise exponential, $\angle(\cdot)$ yields the element-wise argument.

VI. NUMERICAL RESULTS

Simulation results of the effective RCS, σ , defined in (29), are provided in Fig. 5 for the following four scenarios (specific configurations provided in Table I): 1. Anomalous reflection, 2. Specular reflection, 3. Constant spacing, variable number of particles and aperture, and 4. Constant number of particles, variable spacing and aperture.

The simulation results are compared with the effective RCS obtained from an RIS model based on antenna theoretic measures [7], two different RIS models based on physical optics [34, 35], and the RCS of slab of perfect electric conductor (PEC) of the same size. For all scenarios, a square planar array of particles arranged in a equispaced lattice structure is simulated. The array is centered at the origin and aligned with the xy -plane. Unless otherwise stated, the inter-particle spacing is $\Delta = \frac{\lambda}{2}$, the number of particles along the x - and y -axis, $N_x = N_y = 8$, and $\hat{\mathbf{p}}_{\text{in}} = \hat{\mathbf{p}}_{\text{out}} = [1 \ 0 \ 0]^T$. Figures 5a and 5b show the anomalous and specular reflection scenario respectively. In both cases, it is observed that the effective RCS remains almost constant, and does not tend to zero with the projected aperture as ϕ increases. In fact, the maximum effective RCS is observed to be well approximated by $\sigma \approx \pi (3Nk^{-1})^2$ regardless of the angles of illumination and reflection. This fact is in direct disagreement with the models in [7, 34, 35], which are widely assumed in the related literature. Fig. 5c shows an expected linear scaling of the effective RCS with the aperture of the RIS, which is equivalent of a scaling in the number $N = N_x N_y$ of elements squared. Finally, Fig. 5d shows how the effective RCS scales as the aperture of the RIS is squeezed and stretched. Notable is the fact that with a normalized aperture of $\frac{N_x N_y}{16} = 4$, equivalent of a spacing of $\Delta = \frac{\lambda}{4}$, the maintains a RCS of $\sigma \approx 10$ dB while the physical optics models shows a rapid decrease in effective RCS. As the RIS aperture is stretched out, the model shows a peak in the effective RCS at a spacing of $\Delta \approx 0.9\lambda$, after which the effective RCS starts to decrease.

VII. CONCLUSIONS

This work presents a narrowband analysis of single-layer metasurface based RISs, and investigates the different wave interactions that are possible under this architecture while conserving power and ensuring RIS reciprocity.

TABLE I
SIMULATION PARAMETERS

Scenario	$\hat{\mathbf{r}}_{\text{in}}$	$\hat{\mathbf{r}}_{\text{out}}$	Variable
Anomalous reflection	$\begin{bmatrix} 0 \\ -\sin(\phi) \\ -\cos(\phi) \end{bmatrix}$	$\begin{bmatrix} 0 \\ 0 \\ 1 \end{bmatrix}$	$\phi \in [0; \frac{\pi}{2}]$
Specular reflection	$\begin{bmatrix} 0 \\ -\sin(\frac{\phi}{2}) \\ -\cos(\frac{\phi}{2}) \end{bmatrix}$	$\begin{bmatrix} 0 \\ -\sin(\frac{\phi}{2}) \\ \cos(\frac{\phi}{2}) \end{bmatrix}$	$\phi \in [0; \pi]$
Constant spacing	$\sqrt{0.5} \begin{bmatrix} 0 \\ -1 \\ -1 \end{bmatrix}$	$\sqrt{0.5} \begin{bmatrix} 0 \\ -1 \\ 1 \end{bmatrix}$	$N_x, N_y \in [1; 10]$
Constant number of particles	$\sqrt{0.5} \begin{bmatrix} 0 \\ -1 \\ -1 \end{bmatrix}$	$\sqrt{0.5} \begin{bmatrix} 0 \\ -1 \\ 1 \end{bmatrix}$	$\Delta \in [\frac{\lambda}{4}; \lambda]$

The analysis demonstrates that all while conserving power at the element level, it is theoretically possible, using a *single* RIS element, to create; a one-way communication channel, given that the in-and-outgoing directions or polarizations are orthogonal, or at least two orthogonal communication channels without utilizing orthogonal polarizations. This means that the same aperture can be utilized to serve multiple communication links without causing interference.

The analysis also disproves the common assumption that a RIS is capable of doing constant amplitude phase-shifting for all separation angles simultaneously. It investigates the implications of this limitation for a RIS assisted communication scenarios. Due to the lack of constant amplitude phase-shifting, the cascaded channel model, $h = h_1 \phi h_2$, is not valid in multipath scenarios. This has implications for systems relying on signal-space channel estimation, as the channel does not remain deterministic as the phase-shift of an element is changed. However, the analysis also shows that given a sufficiently high number of reconfigurable RIS elements, e.g. 128, the loss in signal power due to this randomness becomes negligible.

For a planar array, the analysis finds that the maximum RCS of a RIS is well approximated by $\sigma \approx \pi (3Nk^{-1})^2$, where N is the total number of elements and λ is the wavelength. A higher frequency thus requires more elements to achieve the same effective RCS and thereby signal power. The simulations shows the effective RCS does not scale with the projected aperture of the RIS, as the effective RCS remains in the same order of magnitude as the angles of incidence and reflection approaches angles parallel to the RIS plane. This is in contrast to what is predicted by the physical optics based models [34, 35], which predicts the effective RCS tending to zero as the angles of incidence and reflection becomes parallel to the RIS plane.

APPENDIX A

RELATIONS AND CONDITIONS FOR POINT ACTORS

This appendix derives conditions for passive point actors and reciprocal point actors. The current distribution for a point actor positioned at \mathbf{x}' is given as

$$\begin{bmatrix} \mathbf{j}(\mathbf{x}) \\ \mathbf{m}(\mathbf{x}) \end{bmatrix} = \delta(\mathbf{x} - \mathbf{x}') \begin{bmatrix} \mathbf{j} \\ \mathbf{m} \end{bmatrix}. \quad (90)$$

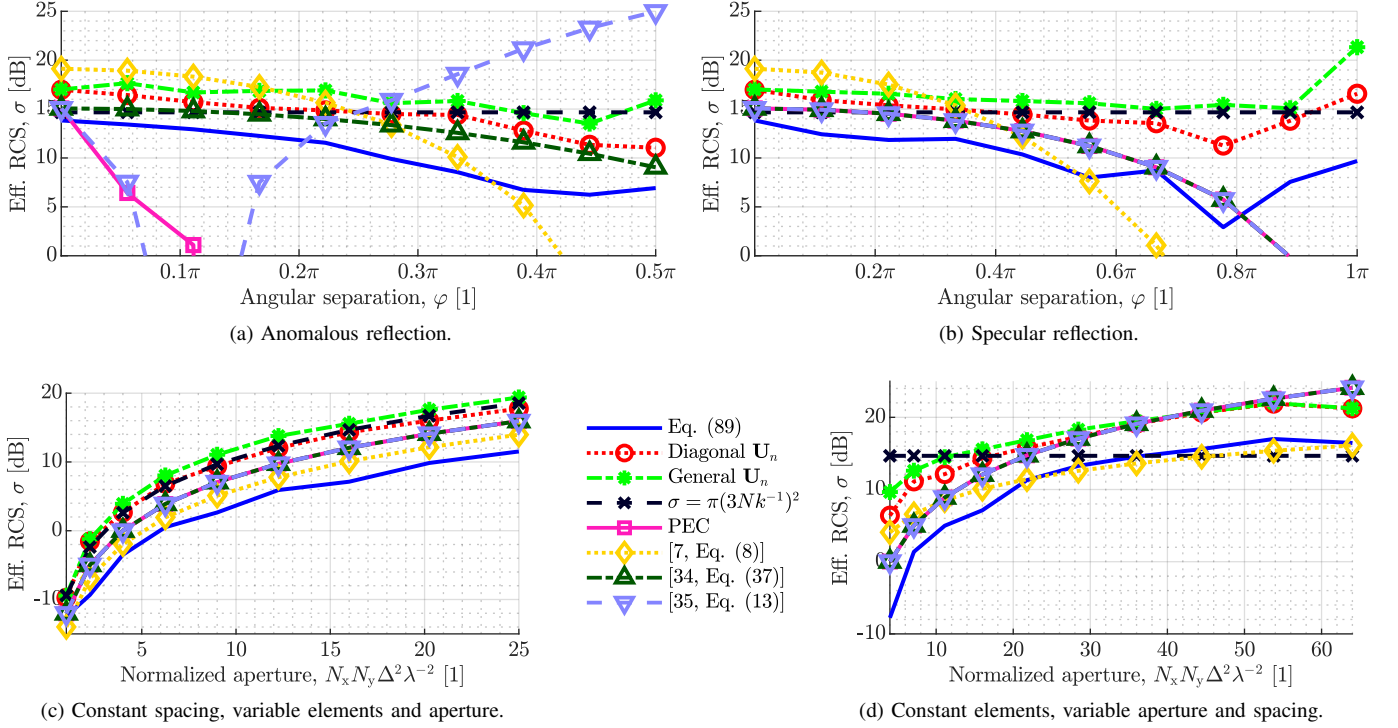


Fig. 5. Simulation results for scenarios one through four.

A. Passive and lossless conditions

For a point scatterer defined by the polarizability matrix \mathbf{X} , being passive implies that the supplied power $P_s \leq 0$, and being lossless implies that the supplied power $P_s \geq 0$. As such, for the point scatterer to be both passive and lossless implies that $P_s = 0$. The time-averaged power *supplied* by the point actor is given as [36, sec. 1.7.3]

$$P_s = \frac{-1}{2} \iiint_V \text{Re} \left\{ \begin{bmatrix} \mathbf{e}(\mathbf{x}) \\ \mathbf{h}(\mathbf{x}) \end{bmatrix}^H \begin{bmatrix} \mathbf{j}(\mathbf{x}) \\ \mathbf{m}(\mathbf{x}) \end{bmatrix} \right\} d\mathbf{x}, \quad (91)$$

$$= \frac{-1}{2} \text{Re} \left\{ \begin{bmatrix} \mathbf{e}(\mathbf{x}') \\ \mathbf{h}(\mathbf{x}') \end{bmatrix}^H \begin{bmatrix} \mathbf{j} \\ \mathbf{m} \end{bmatrix} \right\}. \quad (92)$$

Applying (33) and (37) yields

$$P_s = \frac{-1}{2} \text{Re} \left\{ \begin{bmatrix} \mathbf{e}_a \\ \mathbf{h}_a \end{bmatrix}^H \left(\mathbf{X}^H \mathbf{G} (\mathbf{0}_{3 \times 1})^H \mathbf{X} + \mathbf{X} \right) \begin{bmatrix} \mathbf{e}_a \\ \mathbf{h}_a \end{bmatrix} \right\},$$

$$= \frac{-1}{2} \begin{bmatrix} \mathbf{e}_a \\ \mathbf{h}_a \end{bmatrix}^H \left(\frac{\mathbf{X} + \mathbf{X}^H}{2} + \mathbf{X}^H \mathbf{G}_0 \mathbf{X} \right) \begin{bmatrix} \mathbf{e}_a \\ \mathbf{h}_a \end{bmatrix}. \quad (93)$$

where $\begin{bmatrix} \mathbf{e}_a & \mathbf{h}_a \end{bmatrix}^T$ is the field acting upon the point scatterer and \mathbf{G}_0 is given by (8). The scatterer is lossless and passive, $P_s = 0$, i.e., if and only if (38) holds.

B. Reciprocity conditions

To investigate channel reciprocity, we consider a single point scatterer and two point actors positioned at spatial coordinates \mathbf{x}_0 , \mathbf{x}_1 , and \mathbf{x}_2 respectively. The first point actor carries currents \mathbf{j} and \mathbf{m} which radiates an electromagnetic field. The field is

measured by the other actor along the dimension dictated by the measurement vector \mathbf{a} , yielding the signal h_1 . \mathbf{a} corresponds to an effective gain pattern in conventional antenna theory terms. \mathbf{a} is split into its electric and magnetic parts as $\mathbf{a} = \begin{bmatrix} \mathbf{a}_e & \mathbf{a}_m \end{bmatrix}^T$. Afterwards, the positions are switched and the sign of the effective magnetic currents \mathbf{m} and the magnetic measurement vector \mathbf{a}_m is switched to reverse the direction of radiation and measurement. Repeating the process, yields the measured signal h_2 . h_1 and h_2 are given as

$$h_1 = \begin{bmatrix} \mathbf{a}_e \\ \mathbf{a}_m \end{bmatrix}^T \left(\mathbf{G}(\mathbf{x}_2 - \mathbf{x}_1) + \mathbf{G}(\mathbf{x}_2 - \mathbf{x}_0) \mathbf{X} \mathbf{G}(\mathbf{x}_0 - \mathbf{x}_1) \right) \begin{bmatrix} \mathbf{j} \\ \mathbf{m} \end{bmatrix}, \quad (94)$$

$$h_2 = \begin{bmatrix} \mathbf{a}_e \\ -\mathbf{a}_m \end{bmatrix}^T \left(\mathbf{G}(\mathbf{x}_1 - \mathbf{x}_2) + \mathbf{G}(\mathbf{x}_1 - \mathbf{x}_0) \mathbf{X} \mathbf{G}(\mathbf{x}_0 - \mathbf{x}_2) \right) \begin{bmatrix} \mathbf{j} \\ -\mathbf{m} \end{bmatrix}. \quad (95)$$

For channel reciprocity, we require that the two measured signals are equal, i.e., $h_1 = h_2$. Defining the submatrices of \mathbf{X} according to (42) and exploiting the symmetry of the free space Green's matrix, the conditions for reciprocity yield; $\mathbf{X}_{ee} = \mathbf{X}_{ee}^T$, $\mathbf{X}_{mm} = \mathbf{X}_{mm}^T$, and $\mathbf{X}_{em} = -\mathbf{X}_{me}^T$.

APPENDIX B

UNITARY MATRICES FOR EXAMPLES

For all example matrices, $u_{n,m} = \begin{cases} 0 & n \neq m \\ -1 & n = m \end{cases}$ unless otherwise stated.

- 1) Constant Amplitude phase-shifting for $\varphi = 0$ and $\vartheta = 0$:

$$u_{1,1} = -u_{5,5} = e^{i(\rho + \frac{\pi}{2})}. \quad (96)$$

- 2) Constant Amplitude phase-shifting for $\varphi = \frac{\pi}{2}$ and $\vartheta = 0$:

$$u_{1,1} = e^{i(\rho + \frac{\pi}{2})}, \quad u_{5,5} = 0, \quad u_{6,5} = u_{5,6} = -1. \quad (97)$$

- 3) Constant amplitude phase-shifting for all on-axis angles, orthogonal polarization:

$$\begin{aligned} u_{1,1} &= 0, \quad u_{2,1} = u_{1,2} = -u_{4,1} = u_{4,1} = \frac{\sqrt{2}}{2} e^{i(\rho + \frac{\pi}{2})}, \\ u_{2,2} &= u_{4,2} = -u_{4,4} = -u_{2,4} = \frac{-1}{2}. \end{aligned} \quad (98)$$

- 4) One-way communications for all on-axis angles, orthogonal polarization.

$$\begin{aligned} u_{1,1} &= u_{3,3} = u_{4,4} = 0, \quad u_{2,1} = -u_{4,1} = \frac{\sqrt{2}}{2} e^{i(\rho + \frac{\pi}{2})}, \\ u_{1,3} &= u_{3,4} = -1, \quad u_{2,2} = u_{4,2} = \frac{-\sqrt{2}}{2}. \end{aligned} \quad (99)$$

- 5) Spatial multiplexing, parallel receiver and transmitter:

$$u_{5,5} = u_{6,6} = -i. \quad (100)$$

- 6) Spatial multiplexing, orthogonal receiver and transmitter:

$$\begin{aligned} u_{6,6} &= 1, \quad u_{1,1} = -u_{2,2} = -1 + \frac{\sqrt{3}}{2}, \\ u_{2,1} &= u_{1,2} = \frac{\sqrt{-3+4\sqrt{3}}}{2}. \end{aligned} \quad (101)$$

REFERENCES

- [1] E. Bjornson, H. Wymeersch, B. Matthiesen, P. Popovski, L. Sanguinetti, and E. de Carvalho, "Reconfigurable Intelligent Surfaces: A signal processing perspective with wireless applications," *IEEE Signal Process. Mag.*, vol. 39, no. 2, pp. 135–158, March 2022.
- [2] A. Zappone and M. D. Renzo, "Energy efficiency optimization of reconfigurable intelligent surfaces with electromagnetic field exposure constraints," *IEEE Signal Process. Lett.*, vol. 29, pp. 1447–1451, 2022.
- [3] Y. Yu, J. Wang, X. Zhou, C. Wang, Z. Bai, and Z. Ye, "Review on Channel Estimation for Reconfigurable Intelligent Surface Assisted Wireless Communication System," *Mathematics*, vol. 11, no. 14, p. 3235, Jul. 2023.
- [4] S. Hassouna *et al.*, "A survey on reconfigurable intelligent surfaces: Wireless communication perspective," *IET Communications*, vol. 17, no. 5, pp. 497–537, Mar. 2023.
- [5] E. Björnson and L. Sanguinetti, "Rayleigh fading modeling and channel hardening for reconfigurable intelligent surfaces," *IEEE Wireless Commun. Lett.*, vol. 10, no. 4, pp. 830–834, 2021.
- [6] —, "Power scaling laws and near-field behaviors of massive MIMO and intelligent reflecting surfaces," *IEEE Open J. Commun. Soc.*, vol. 1, pp. 1306–1324, 2020.
- [7] W. Tang *et al.*, "Wireless Communications With Reconfigurable Intelligent Surface: Path Loss Modeling and Experimental Measurement," *IEEE Trans. Wireless Commun.*, vol. 20, no. 1, pp. 421–439, Jan. 2021.
- [8] R. J. Williams, E. de Carvalho, and T. L. Marzetta, "A Communication Model for Large Intelligent Surfaces," in *2020 IEEE Int. Conf. Commun. Workshops (ICC Workshops)*. Dublin, Ireland: IEEE, Jun. 2020, pp. 1–6.
- [9] M. Di Renzo, F. H. Danufane, and S. Tretyakov, "Communication Models for Reconfigurable Intelligent Surfaces: From Surface Electromagnetics to Wireless Networks Optimization," *Proc. IEEE*, vol. 110, no. 9, pp. 1164–1209, Sep. 2022.
- [10] K. Achouri and O. J. F. Martin, "Fundamental Properties and Classification of Polarization Converting Bianisotropic Metasurfaces," *IEEE Trans. Antennas Propag.*, vol. 69, no. 9, pp. 5653–5663, Sep. 2021.
- [11] K. Achouri and C. Caloz, *Electromagnetic Metasurfaces: Theory and Applications*. John Wiley & Sons, 2021.
- [12] G. Gradoni and M. Di Renzo, "End-to-end mutual coupling aware communication model for reconfigurable intelligent surfaces: An electromagnetic-compliant approach based on mutual impedances," *IEEE Wireless Commun. Lett.*, vol. 10, no. 5, pp. 938–942, 2021.
- [13] K. Konno, S. Terranova, Q. Chen, and G. Gradoni, "Generalized impedance model of wireless links assisted by reconfigurable intelligent surfaces," *IEEE Trans. Antennas Propag.*, vol. 72, no. 10, pp. 7691–7699, 2024.
- [14] X. Qian and M. D. Renzo, "Mutual Coupling and Unit Cell Aware Optimization for Reconfigurable Intelligent Surfaces," *IEEE Wireless Commun. Lett.*, vol. 10, no. 6, pp. 1183–1187, Jun. 2021.
- [15] A. Abrardo, D. Dardari, M. Di Renzo, and X. Qian, "MIMO interference channels assisted by reconfigurable intelligent surfaces: Mutual coupling aware sum-rate optimization based on a mutual impedance channel model," *IEEE Wireless Commun. Lett.*, vol. 10, no. 12, pp. 2624–2628, 2021.
- [16] H. E. Hassani *et al.*, "Optimization of RIS-aided MIMO—a mutually coupled loaded wire dipole model," *IEEE Wireless Commun. Lett.*, vol. 13, no. 3, pp. 726–730, 2024.
- [17] S. Shen, B. Clerckx, and R. Murch, "Modeling and Architecture Design of Reconfigurable Intelligent Surfaces Using Scattering Parameter Network Analysis," *IEEE Trans. Wireless Commun.*, vol. 21, no. 2, pp. 1229–1243, Feb. 2022.
- [18] S. Abeywickrama, R. Zhang, Q. Wu, and C. Yuen, "Intelligent Reflecting Surface: Practical Phase Shift Model and Beamforming Optimization," *IEEE Trans. Commun.*, vol. 68, no. 9, pp. 5849–5863, Sep. 2020.
- [19] J. A. Nossek, D. Semmler, M. Joham, and W. Utschick, "Physically consistent modeling of wireless links with reconfigurable intelligent surfaces using multiport network analysis," *IEEE Wireless Commun. Lett.*, vol. 13, no. 8, pp. 2240–2244, 2024.
- [20] M. Nerini, S. Shen, H. Li, M. Di Renzo, and B. Clerckx, "A universal framework for multiport network analysis of reconfigurable intelligent surfaces," *IEEE Trans. Wireless Commun.*, vol. 23, no. 10, pp. 14575–14590, 2024.
- [21] M. Nerini and B. Clerckx, "Physically Consistent Modeling of Stacked Intelligent Metasurfaces Implemented with Beyond Diagonal RIS," Feb. 2024, arXiv:2402.12602 [cs, eess, math].
- [22] K. Achouri, M. A. Salem, and C. Caloz, "General Metasurface Synthesis Based on Susceptibility Tensors," *IEEE Trans. Antennas Propag.*, vol. 63, no. 7, pp. 2977–2991, Jul. 2015.
- [23] J. An, M. Di Renzo, M. Debbah, and C. Yuen, "Stacked intelligent metasurfaces for multiuser beamforming in the wave domain," in *ICC 2023 - IEEE Int. Conf. Commun.*, 2023, pp. 2834–2839.
- [24] C. A. Balanis, *Antenna theory: analysis and design*, 4th ed. Hoboken, New Jersey: Wiley, 2016.
- [25] A. F. Molisch, *Wireless communications*, 2nd ed. Chichester, West Sussex, U.K: Wiley : IEEE, 2011, oCLC: ocn613645390.
- [26] J. D. Jackson, *Classical electrodynamics*, 3rd ed. New York: Wiley, 1999.
- [27] R. E. Collin, *Field theory of guided waves*, 2nd ed. New York: IEEE Press, 1991.
- [28] V. Yatsenko and S. M. S. Tretyakov, "Electromagnetic Interaction of Parallel Arrays of Dipole Scatterers," *Progress In Electromagnetics Research*, vol. 25, pp. 285–307, 2000.
- [29] L. Crone, "Second order adjoint matrix equations," *Linear Algebra and its Applications*, vol. 39, pp. 61–71, 1981.
- [30] J. D. Parsons, *The mobile radio propagation channel*, 2nd ed. Chichester : New York: J. Wiley, 2000.
- [31] T. Abrudan, J. Eriksson, and V. Koivunen, "Conjugate gradient algorithm for optimization under unitary matrix constraint," *Signal Processing*, vol. 89, no. 9, pp. 1704–1714, 2009.
- [32] N. Boumal, B. Mishra, P.-A. Absil, and R. Sepulchre, "Manopt, a Matlab toolbox for optimization on manifolds," *Journal of Machine Learning Research*, vol. 15, no. 42, pp. 1455–1459, 2014. [Online]. Available: <https://www.manopt.org>
- [33] A. Hjørungnes, *Complex-Valued Matrix Derivatives: With Applications in Signal Processing and Communications*, 1st ed. USA: Cambridge University Press, 2011.
- [34] F. H. Danufane, M. D. Renzo, J. De Rosny, and S. Tretyakov, "On the Path-Loss of Reconfigurable Intelligent Surfaces: An Approach Based on Green's Theorem Applied to Vector Fields," *IEEE Trans. Commun.*, vol. 69, no. 8, pp. 5573–5592, Aug. 2021.
- [35] V. Degli-Esposti, E. M. Vitucci, M. D. Renzo, and S. A. Tretyakov, "Reradiation and Scattering From a Reconfigurable Intelligent Surface: A General Macroscopic Model," *IEEE Trans. Antennas Propag.*, vol. 70, no. 10, pp. 8691–8706, Oct. 2022.
- [36] C. A. Balanis, *Advanced engineering electromagnetics*, 2nd ed. Hoboken, N.J: John Wiley & Sons, 2012.